Magnetic properties of early Pliocene sediments from IODP Site U1467 (Maldives platform) reveal changes in the monsoon system

Citation for published version:
Lanci, L, Zanella, E, Jovane, L, Galeotti, S, Alonso-garcía, M, Alvarez-zarikian, CA, Bejugam, NN, Betzler, C, Bialik, OM, Blättler, CL, Eberli, GP, Guo, JA, Haffen, S, Horozal, S, Inoue, M, Kroon, D, Laya, JC, Mee, ALH, Lüdmann, T, Nakakuni, M, Niino, K, Petruny, LM, Pratiwi, SD, Reijmer, JJG, Reolid, J, Slagle, AL, Sloss, CR, Su, X, Swart, PK, Wright, JD, Yao, Z & Young, JR 2019, 'Magnetic properties of early Pliocene sediments from IODP Site U1467 (Maldives platform) reveal changes in the monsoon system', *Palaeogeography, Palaeoclimatology, Palaeoecology*, vol. 533, pp. 109283. https://doi.org/10.1016/j.palaeo.2019.109283

Digital Object Identifier (DOI):
10.1016/j.palaeo.2019.109283

Link:
Link to publication record in Edinburgh Research Explorer

Document Version:
Peer reviewed version

Published In:
Palaeogeography, Palaeoclimatology, Palaeoecology

Manuscript Details

Manuscript number	PALAEO_2019_133_R1
Title	Magnetic properties of Early Pliocene sediments from IODP Site U1467 (Maldives platform) reveal changes in the monsoon system
Article type	Research Paper

Abstract

We report a study of the magnetic stratigraphy and the anisotropy of isothermal remanent magnetization of Pliocene sediments from IODP Site U1467 drilled in the Maldives platform (Indian Ocean) during Exp. 359. Magnetic stratigraphy gives a precise record of geomagnetic reversals of the early Pliocene from approximately 5.3 Ma to 3.1 Ma providing a detailed age model in an interval, where the biostratigraphic record was scarce. Anisotropy of isothermal magnetization provides data on strength and direction of bottom current during the early Pliocene. The strength of bottom currents recorded by the anisotropy parameter P', shows a prominent increase at about 4.2 Ma and the currents direction is consistent with that of modern instrumental measurements. Since bottom currents in the Maldives are driven by the monsoon, we speculate that the 4.2 Ma increase of bottom currents could mark the onset of the present-day setting, probably related to the coeval uplift phase of the Himalayan plateau.

Keywords	Pliocene magnetic stratigraphy; Anisotropy of isothermal remanent magnetization; Currents strength; Monsoon
Manuscript region of origin	Europe

Corresponding Author	Luca Lanci
Corresponding Author's Institution	University of Urbino
Order of Authors	Luca Lanci, Elena Zanella, Luigi Jovane, Simone Galeotti, Montserrat Alonso-García, Carlos Alvarez-Zarikian, Christian Betzler, Or Bialik, Clara Blättler, Gregor Eberli, Junhua Guo, Sébastien Haffen, Senay Horozal, Mayuri Inoue, Dick Kroon, Juan Carlos Laya, Anna Ling, Thomas Lüdmann, Masatoshi Nakakuni, Nagender Nath Bejugam, Kaoru Niino, Loren M. Petruny, Santi D. Pratiwi, John J. G. Reijmer, Jesús Reolid, Angela L. Slagle, Craig R. Sloss, Xiang Su, Peter K. Swart, James D. Wright, Zhengquan Yao, Jeremy R. Young

Suggested reviewers	Ann Hirt, Josep Pares, Christopher Lepre, Edoardo Dallanave, Giovanni Muttoni

Submission Files Included in this PDF

File Name [File Type]

1467-cover.docx [Cover Letter]

Responce to reviewers.docx [Response to Reviewers]

1467-Revised ms with ma changes.docx [Revised Manuscript with Changes Marked]

1467-highlights.docx [Highlights]

Graphical abstract.PDF [Graphical Abstract]

1467-manuscript-revised.docx [Manuscript File]

Fig1.map.PDF [Figure]

Fig2-IRM acquisition.pdf [Figure]

Fig3-z_plot.pdf [Figure]

Fig4-Jelinek plot.pdf [Figure]

Fig5-VGP+dir mod.pdf [Figure]

Fig6-Age model + bio.pdf [Figure]

Fig7-AIRM stereo.pdf [Figure]

Fig8-AIRM_logs.pdf [Figure]

1467-tables.docx [Table]

Submission Files Not Included in this PDF

File Name [File Type]

Bata in Brief.zip [Data in Brief]

To view all the submission files, including those not included in the PDF, click on the manuscript title on your EVISE Homepage, then click 'Download zip file'.

Research Data Related to this Submission

Data set https://data.mendeley.com/datasets/8383kp7vsb/draft?a=9687bfa8-8328-4ff7-9cc5-4538f2256ff0

Data for: Magnetic properties of Early Pliocene sediments from IODP Site U1467 (Maldives platform) reveal changes in the monsoon system

Paleomagnetic and rock-magnetic data from IODP Site U1467 from "Magnetic properties of Early Pliocene sediments from IODP Site U1467 (Maldives platform) reveal changes in the monsoon system" by L. Lanci, E. Zanella and Exp. 359 members

Luca Lanci
Dept. of Pure and Applied Science
Università degli Studi di Urbino "Carlo Bò"
Via S. Chiara 27
I-61029 Urbino (PU)
Italy
email: luca.lanci@unirb.it

July 10, 2019

Dr. Thierry Correge
Editor of Palaeogeography Palaeoclimatology Palaeoecology

Dear Sir,

I wish to submit the revised version of the manuscript titled "*Magnetic properties of Early Pliocene sediments from IODP Site U1467 (Maldives platform) reveal changes in the monsoon system*" by L. Lanci, et al, to be considered for publication in Palaeogeography Palaeoclimatology Palaeoecology.

I believe we have answered properly to all reviewers' questions and suggestions, which were very useful, as detailed in the file "response to reviewers". Major changes include an amended interpretation of the paleo-currents directions and redrawn figures, that we hope became more attractive. A new co-author has been added, who contributed to the paleoceanographic interpretation.

We hope that the manuscript could be of interest for Paleo3.

Sincerely,

Luca Lanci.

Magnetic properties of early Pliocene sediments from IODP Site U1467 (Maldives platform) reveal changes in the monsoon system, by Lanci et al.

Response to reviewers

Reviewer #1

Q:
Depths throughout the MS:
Since 2011 the depth of IODP cores and samples is expressed as CSF-A, CSF-B, and CCSF (not mbsf or mcd). Please check the guidelines: https://www.iodp.org/policies-and-guidelines/142-iodp-depth-scales-terminology-april-2011/file.

In this regards, the data given in the online Table (U1467_data.xclx) are not correct and therefore not acceptable (only for practical reasons: every specimen should be traceable). The extended sample code should be in the form of (e.g.) 359U1467B12H1W060/062. This information is given (almost in the complete form) in the NRM direction table BUT NOT in the anisotropy table, where the Hole is not indicated.

The list of samples MUST be associated with the CSF-A value (former mbsf), and this value is missing in both tables.

A: We have changed all depth to meter CSF-A as requested by the reviewers. This apply to figures, tables and to the Excel data sheet.

Q: *Furthermore, there is a major issue regarding the depth in the figures. The magnetostratigraphy presented in figure 6 does not fit with the depth shown in figure 8 (anisotropy data). For example the deepest normal magnetic polarity interval N6 is at about 260–280 m in Fig. 6 but much shallower in Fig. 8, and the scale is the same (mbsf). Even if this should not affect the age of bottom current inception as interpreted from the AIRM data, it must be reviewed.*

A: We acknowledge that there was a mistake in pasting the black and white column into the figure of anisotropy data (former Fig. 6). This mistake have been corrected. Moreover, the new figure (now Fig. 8) has been redrawn in a (hopefully) more attractive format, a smoothed line that shows the data trends was added as suggested by reviewer #1. Moreover, to increase the information shown in the figure we also introduced a color code for the anisotropy shape parameter (T).

Q:
Anisotropy of IRM:
The model put forward in this MS is based on the AIRM and its mathematical expression P'. The background to obtain P' is limited to the laboratory procedure (actually not very well explained, see comment on PDF), and it is

called out in line 313 simply as "anisotropy parameter" without any reference or explanation.

I presume it is the 'corrected anisotropy degree' of Jelínek (1981), usually applied to AMS, but I would like to see the equation in the MS, since there is often confusion in the literature about the names of anisotropy parameters. There is no other information regarding the shape of the AIRM tensor, neither related to each sample nor to the mean one. The shape could be easily quantified by the "T" factor of Jelínek (1981)(or maybe, even better with the bootstrap approach of Constable and Tauxe (1990)?). The statistic approach used in the last figure is not indicated, and there is a legend without unit.

A: We have amended the definition of the parameter used in the description of anisotropy. The formula for the corrected anisotropy degree (P') and the shape parameter (T) were provided together with the reference.
A new figure (Fig. 4) with a so-called Jelinek plot, to illustrate the shape of the anisotropy ellipsoids, was added to the manuscript as suggest by reviewer #1 in the annotated ms.

Q: *Furthermore, even if P' is much lower in the "pre-monsoon inception" part of the section, it is important to show a stereographic projection of the eigenvectors, for comparison with the upper part. The distribution of the minimum eigenvector could be elongated NE-SW also before the inception of the monsoon-driven bottom current regime.*

What about also defining a P' minimum value under which the anisotropy is statistically meaningless? It could strengthen the interpretation.

A: We show the stereographic projection of the low P' data as requested in the new Figure 7. Following suggestions we have defined a P' value below which the anisotropy do not have statistically significant orientations and divided the specimens in two sets according to this value. The paleo-currents interpretation was improved by evaluating the AIRM pattern of each sample to infer the current directions that are reported in a circular plot for both sets of samples with high P' and low P'. A statistical test have been applied to ensure that the set with high P' had grouped direction and that the set with lower P' had uniformly distributed directions. Mean directions were calculated only for the set with high P' using Von Mises statistics. Results are shown in the new figure 7.

Other changes following suggestions on the annotated ms.:

As requested in the annotated ms., in section "*4.2. Anisotropy of the IRM*" we have expanded the paleocenographic explanation of possible monsoon effect on the bottom currents. Admittedly the arguments was very briefly explained even in the cited literature and certainly deserved a better explanation.

Online Table (U1467_data.xclx):

The table has been reviewed as suggested, in particular sample code for anisotropy were corrected, sample depth was reported in m CSF-A and MDF calculation were added to the table. The complete set of data is available in the excel file.

Figure changes

Figure 2:
Figure 2 was redrawn reporting the specimens code and adding a second panel with the distribution of the median destructive field of the NRM, as suggest by reviewer #1 in the annotated ms.

Figure 3:
We added the labels with demagnetizing fields as requested by reviewer #1 in the annotated ms.

New figure 4:
A new figure (Fig. 4) with a so-called Jelinek plot, to illustrate the shape of the anisotropy ellipsoids, was added to the manuscript as suggest by reviewer #1 in the annotated ms.

New Figure 5:
Figure 5 (former Figure 4) was redrawn reporting the core photographs and the lithostratigraphic units as requested by reviewer #1 in the annotated ms. Moreover, following the suggestions on the annotated ms, were also reported the positions of all measured specimens in order to get a more precise idea of the success rate for magnetostatigraphy.

New figure 7:
Figure 7 was completely redrawn as described above.

New figure 8 (former figure 6):
The new figure 8 have has been redrawn as described above.

Reviewer #2

Q: *First of all, given that the journal has a rather wide scope in paleoclimatology, paleogeography, the authors need to explain a bit better the basis and the parameters that are used in magnetic anisotropy. For example, in line 289 they referred to Imax and Imin, but do not explain what they mean- They do not represent "preferred orientations" (line 289), but the inclination of the maximum and minimum axes of the AIRM matrix.*

A: We have changed I_{max} and I_{min} to I_1 and I_3, which is a "standard" notation for principal axis of AIRM, and defined them as eigenvectors of the IRM anisotropy tensor. We also gave a description of their geological interpretation.

Q: *More confusing is the interpretation of Figure 7 (a key part of the paper!): Where is mean direction of 134/00 seen in the stereonet? What do they mean by "elongation axis Imax"? (the scatter / grouping of the individual axes?). Also, the same figure contains two types of planes (in blue and red)- what do they mean? And the colored bar on the side?*

A: We have amended the interpretation of the paleocurrent data and Figure 7 has been completely redrawn following also suggestions of reviewer #1. We hope the new figure and interpretation answer these questions.

Q: *How can they assert that a "the averaged direction of foliation planes" is 137 N? What are the white dots represented? (I assume the axes if minimum ARM, but both the legend and the text fail to explain so). If anything, I can see the NE-SW trend, which would correspond to an azimuth of about 40 deg. So, in general, the paragraph from lines 315 to 319 is rather confusing. The authors do a great job describing possible scenario for the AIRM axes distribution (imbrications, flow-transverse fabrics, flow-aligned fabric, etc.) yet they fail in stating in a clear way which case is what they find and WHY they think so.*

So, notice that my main comment is not merely about complementing the legend of such figure, but explaining how the authors go from the basis of the method (lines 294 to 305 to the interpretation of the observed fabric (lines 315 to 322). This part is critical to the paper.

A: As described above, in order to answer this comment and a similar request from reviewer #1, the AIRM interpretation have been improved and the results illustrated in new Figure 7.

Q: *Last, but not least, there is a change (stratigraphically upwards) in magnetite concentration, as shown by the increase of the IRM intensity. Such change is accompanied by a slight increase of the anisotropy degree (possible proxy for the strength of the bottom current). The authors interpret such change in anisotropy as the initiation of the monsoon. If that is the case, wouldn't you expect an increase of dust and terrigenous flux from the continent as well? An increase on terrigenous influx, as one would expect, should be conducive to an increase of magnetite as well. So such seemingly contradiction needs to be explained.*

A: This question was already explained in the first submission, we have slightly changed it as follow: "From the sedimentological point of view, the decrease of IRM is interpreted as a consequence of changes in the sediment transport mechanism -controlled by wind driven currents- that transferred the sediments and the single-domain magnetite, possibly of biogenic origin, from the shallow platform to the deeper water of Site U1467 (Lüdmann et al., 2013). This process is accelerated by the increased monsoon strength starting at 168 m CSF-A depth."

Magnetic properties of early~~Early~~ Pliocene sediments from IODP Site U1467 (Maldives platform) reveal changes in the monsoon system

Luca Lanci[1,2], Elena Zanella[2,3], Luigi Jovane[4], Simone Galeotti[1], Montserrat Alonso-García[5,6], Carlos A. Alvarez-Zarikian[7], Christian Betzler[8], Or M. Bialik[9], Clara L. Blättler[10], Gregor P. Eberli[11], Junhua Adam Guo[12], Sébastien Haffen[13], Senay Horozal[14], Mayuri Inoue[15], Dick Kroon[16], Juan Carlos Laya[17], Anna Ling Hui Mee[11], Thomas Lüdmann[8], Masatoshi Nakakuni[18], Nagender Nath Bejugam[19], Kaoru Niino[20], Loren M. Petruny[21], Santi D. Pratiwi[22], John J. G. Reijmer[23], Jesús Reolid[24], Angela L. Slagle[25], Craig R. Sloss[26], Xiang Su[27], Peter K. Swart[11], James D. Wright[28], Zhengquan Yao[29, 30], Jeremy R. Young[31]

1) Department of Pure and Applied Science, University of Urbino, Via S. Chiara 27, 61029 Urbino, Italy.

2) Alpine Laboratory of Paleomagnetism ALP - CIMaN, Via G.U. Massa 6, 12016 Peveragno, Italy

3) Department of Earth Sciences, University of Turin, Via Valperga Caluso 35, 10125 Turin, Italy

4) Instituto Oceanográfico da Universidade de São Paulo, Praça do Oceanográfico, 191, São Paulo, SP 05508-120, Brazil.

5) Divisão de Geologia e Georecursos Marinhos, Instituto Portugues do Mar e da Atmosfera (IPMA), Avenida de Brasilia 6, 1449-006 Lisbon, Portugal.

6) Centro de Ciencias do Mar (CCMAR), Universidade do Algarve, Faro, Portugal.

7) International Ocean Discovery Program, Texas A&M University, 1000 Discovery Drive, College Station, TX 77845, USA.

8) Institute for Geology, CEN, University of Hamburg, Bundesstrasse 55, 20146 Hamburg, Germany.

9) Dr. Moses Strauss Department of Marine Geosciences, The Leon H. Charney School of Marine Sciences, University of Haifa, 31905 Carmel, Israel.

10) Department of the Geophysical Sciences,~~Geosciences, Princeton~~ University of Chicago, 5734 S. Ellis Ave., Chicago, IL 60637~~, Guyot Hall, Princeton, NJ 08544~~, USA.

11) Department of Marine Geosciences, Department of Marine Geosciences, Rosenstiel School of Marine and Atmospheric Science, University of Miami, Miami, FL 33149, USA.

12) Department of Geological Sciences, California State University Bakersfield, 9001 Stockdale Highway, Bakersfield, CA 93311, USA.

13) Physical Properties Specialist, Ecole Nationale Superieure de Geologie, Universite de Lorraine, 2 rue du Doyen Marcel Roubault, 54501 Vandoeuvre-les-Nancy, France.

14) Petroleum and Marine Research Division, Korea Institute of Geoscience and Mineral Resources (KIGAM), Gwahang-no 124, Yuseong-gu, Daejeon 305-350, Korea.

15) Graduate School of Natural Science and Technology, Okayama University, 3-1-1 Tsushima-naka, Okayama 700-8530, Japan.

16) Department of Geology and Geophysics, University of Edinburgh, Grant Institute, The King's Buildings, West Mains Road, Edinburgh EH9 3JW, UK.
17) Department of Geology and Geophysics, Texas A&M University, Mail Stop 3115, College Station, TX 77843-3115, USA.
18) Department of Environmental Engineering for Symbiosis, Soka University, 1-236 Tangi-cyo, Hachioji-shi, Tokyo 192-0003, Japan.
19) Geological Oceanography Division, CSIR-National Institute of Oceanography, Dona Paula, Goa 403004, India.
20) Graduate School of Science and Engineering, Yamagata University, 1-4-12 Kojirakawa-machi, Yamagata City 990-8560, Japan.
21) Environmental Science and Policy Department, George Mason University, David King Hall Rm 3005, MSN 5F2, 4400 University Drive, Fairfax, VA 22030-4444, USA.
22) Department of Geosciences, Geotechnology and Materials Engineering for Resources, Akita University, 1-1 Teagata-Gakuencho, Akita 010-8502, Japan.
23) College of Petroleum Engineering and Geosciences, King Fahd University of Petroleum and Minerals, Dhahran 31261, Saudi Arabia.
24) Departamento de Estratigrafía y Paleontología, Universidad de Granada, Avenida de La Fuente Nueva S/N, 18071, Granada, Spain.
25) Lamont-Doherty Earth Observatory, Columbia University, Borehole Bldg. 61 Route 9W, Palisades, NY 10964, USA.
26) Earth and Environmental Sciences, University of Technology Queensland, R-Block 317, 2 George Street, Brisbane, QLD 4001, Australia.
27) Key Laboratory of Marginal Sea Geology, South China Sea Institute of Oceanology, Chinese Academy of Sciences, 164 West Xingang Road, Guangzhou 510301, People's Republic of China.
28) Department of Geological Sciences, Rutgers, The State University of New Jersey, 610 Taylor Road, Piscataway, NJ 08854-8066, USA.
29) Department of Marine Geology, First Institute of Oceanography (FIO) State Oceanic Administration (SOA), #6 Xian Xia Ling Road, Qingdao 266061, Shandong Province, People's Republic of China.
30) Laboratory for Marine Geology, Qingdao National Laboratory for Marine Science and Technology, Qingdao, People's Republic of China.
31) Department of Earth Sciences, University College London, Gower Street, London WC1E 6BT, UK.

Abstract

We report a study of the magnetic stratigraphy and the anisotropy of isothermal remanent magnetization of Pliocene sediments from International Ocean Discovery Program (IODP) Site U1467 drilled in the Maldives platform (Indian Ocean) during Exp. 359. Magnetic stratigraphy gives a precise record of geomagnetic reversals of the early Pliocene from approximately 5.3 Ma to 3.1 Ma providing a detailed age model in an interval~~,~~ where the biostratigraphic record is~~was~~ scarce. We use the anisotropy ~~Anisotropy~~ of isothermal remanent magnetization (AIRM) to investigate the statistical orientation of fine magnetic particles and provide~~provides~~ data on the strength and direction of bottom currents~~current~~ during the early Pliocene. The strength of bottom currents recorded by the AIRM~~anisotropy parameter P'~~, shows a prominent increase at the top of Chron C3n.1n (about 4.2 Ma), and the current~~currents~~ direction (NE - SW) is consistent with that of modern instrumental measurements. Since bottom currents in the Maldives are driven by the monsoon, we speculate that the 4.2 Ma increase of bottom currents could mark the onset of the present-day setting, probably related to the coeval uplift phase of the Himalayan plateau.

Keywords: Paleomagnetism; Pliocene magnetic stratigraphy; Anisotropy of isothermal remanent magnetization; Currents strength; Monsoon

1. Introduction

Wind-induced currents are an important factor controlling the sedimentation in the~~The~~ Maldives archipelago where they regulate sediment transport~~the sediments transportation~~ from the atoll to the deeper part of the platform as well as the geometry of the sedimentary bodies (e.g., Betzler et al., 2009; Lüdmann et al., 2013; Betzler et al., 2016b~~2016~~). The onset of these current-driven drift deposits has been related to the increase of monsoon activity starting in the middle Miocene (Betzler et al., 2016b~~2016~~). In this paper we report results from paleo and rock-magnetic analyses from International Ocean Discovery Program (IODP) Site U1467 aiming to improve the Pliocene age model and investigate the variations of bottom current strength.

Site U1467 (4° 51.0155' ~~0155°~~N and 73° 17.0204' ~~0204°~~E) was drilled in the Inner Sea of the~~The~~ Maldives archipelago~~atoll~~ (Indian Ocean) during IODP Expedition 359 at a water depth of 487.4 m (Betzler et al., 2017) in a distal position compared to the platform margins and moats (Fig. 1). Site U1467 showed nearly horizontally layered seismic reflections of the so-called drift sequences (Betzler et al., 2013, Lüdmann et al., 2013; Wunsch et al., 2017) with no truncations and no indications of mass wasting from the adjacent platform margin. Shipboard analysis suggested that Site U1467 provided a complete and undisturbed succession of all drift sequences from the Late Miocene (Betzler et al., 2017) with good potential for paleoceanographic and paleoclimatic studies. In particular the drift succession, from mid-Miocene to recent, contains several sequences that are potentially related to fluctuations in the monsoon-driven current system. Dating these sequences can yield the ages of changes in the strength and direction of the currents.

The paleomagnetic~~Paleomagnetic~~ analysis in~~of~~ this study provides~~provide~~ the magnetostratigraphic age of the upper portion of Site U1467 that was sampled with advanced piston coring (APC), and uses the anisotropy of the isothermal remanent magnetization (AIRM) to investigate the statistical orientation of fine magnetic particles aiming to provide a sedimentological record of direction and strength of bottom currents. ~~The drift deposition has been related to an increased monsoon strength since the middle Miocene (Betzler et al., 2016) and, although there is not a direct effect of winds on currents below the thermocline depth, there are ample sedimentological evidence that sea-bottom currents in the Maldives are driven by the monsoon (e.g., Betzler et al., 2009, Lüdmann et al., 2013, Betzler et al., 2016).~~

Shipboard paleomagnetic measurements of Site U1467 (Betzler et al., 2016, Betzler et al., 2017) gave poor results because of a combination of two factors: (i) the very low concentration of magnetic minerals in carbonate platform sediments, which resulted in a very weak natural remanent magnetization (NRM) and (ii) a strong magnetic contamination of the cores due to metallic particles presumably originating from the drilling pipes. The contamination covered the original weak paleomagnetic signal of the sediment preventing any valuable measurements with the shipboard pass-through technique that measures half-cores. Measurements of individual~~single~~ 7 cm^3 box-samples, taken from the inner part of the core, performed aboard, did not show signs of ~~a~~ significant contamination suggesting that it was restricted to the outer part of the cores. Unfortunately, the NRM ~~natural remanent magnetization (NRM)~~ of these specimens, ranging from ca. 1 x 10^{-5} A/m to 1 x 10^{-4} A/m, was too weak to be measured reliably using the JR-6 spinner magnetometer available on the Joides Resolution. However, the NRM of the supposedly uncontaminated box-samples is within the range of sensitivity of a DC-SQUIDS cryogenic magnetometer, and this provided the motivation to collect and measure 580 standard sediment specimens with the aim to obtain a reliable magnetic stratigraphy of Site U1467.

2. Material and sampling

Standard paleomagnetic~~Paleomagnetic standard~~ specimens (Natsuhara-Giken sampling~~2x2 plastic~~ cubes, with a volume of 7 cm^3) were collected in the upper part of Site U1467 from core sections 359-U1467B-11H to 359-U1467B-34H~~33H~~ and from 359-U1467C-10H to 359-U1467C-17H, corresponding to 84 m to 302 m core depth ~~from 84 meter composite depth (mcd)~~ below sea floor (CSF-A),~~to 330 mcd,~~ at the Gulf Coast Repository ~~(GCR)~~ at Texas A&M University. Specimens were sampled only from azimuthally-oriented APC~~advanced piston~~ cores~~, (APC),~~ since information on core orientation is essential for paleomagnetic studies at equatorial latitudes~~latitude~~ such as for~~that of~~ Site U1467.

According to the shipboard sedimentology, the studied part of Site U1467 was divided into three main lithostratigraphic units (Betzler et al., 2017). The uppermost Unit I was recovered in the top 110 m CSF-A~~mcd~~ and consists of unlithified, foraminifer-rich wackestone to packstone with a predominance of very fine- to fine-grained wackestone. Unit II extends from ca. 110 m ~~mcd~~ to 215 m CSF-A~~mcd~~; it comprises ~~the~~ late Pliocene sediments and is characterized by interlayered unlithified and partially lithified planktonic foraminifera~~foraminifer~~–rich wackestone and mudstone with pteropods and particulate organic matter. Unit III, which extends from 215 m~~mcd~~ to 303 m CSF-A~~mcd~~, consists of partially lithified very fine–grained mudstone to wackestone with a dominance of wackestone. The sediment contains abundant planktonic foraminifera~~foraminifers~~; echinoid spines and sponge spicules are common while benthic foraminifera~~foraminifers~~ are rare. Microfossil~~Microfossils~~ preservation throughout Units III and most of Unit II was generally poor to moderate, and in particular the interval from ca. 150 m~~mcd~~ to 300 m~~mcd~~ yields no biostratigraphic ages. The interval chosen for paleomagnetic study was also intended to cover~~covers~~ this interval with poor or absent biostratigraphy~~biostratigraphic record~~.

3. Paleomagnetic analysis

3.1. Isothermal remanent magnetization

Magnetic mineralogy was investigated by acquisition of isothermal remanent magnetization (IRM) in a set of pilot specimens. IRM was acquired in 12 stepwise increasing fields from 0.03 T to 1 T, induced using a ASC pulse magnetizer (Fig. 2a). Results indicate that all measured specimens are characterized by the ~~only~~ presence of only low-coercivity magnetic minerals~~mineral~~ that saturate in fields between 100 mT and 250 mT. These coercivities are below the maximum coercivity of uniaxial magnetite (e.g. Tauxe , 2002) and suggest ~~(Fig. 2). This suggests~~ a rather homogeneous mineralogy made of ferromagnetic minerals such as magnetite (or maghemite) without any significant presence of diagenetic iron sulphides~~sulphates~~ that can be distinguished from their higher coercivity (e.g., Tauxe, 2002).~~.~~

The saturated isothermal remanent magnetization is relatively weak, as often found in carbonate sediments, because of the low concentration of ferrimagnetic minerals. It ranges~~Its variations range~~ from 1.0x10^{-3} to 3.7x10^{-2} A/m, suggesting a wide~~comparable~~ variability in the concentration of magnetic minerals.

3.2. Natural remanent magnetization

The pass-through shipboard measurements of the NRM showed a huge scope of values with ~~NRM~~ intensity ranging from 5 x 10^{-6} A/m to 1 x 10^{-1} A/m along the same core and with a strong downcore decreasing trend (Betzler et al., 2017). This was interpreted as the consequence of steel contamination most likely originating from worn off drill pipes. The bottom part of each APC core, which were the least contaminated, exhibited NRM values ranging from ca. 5 x 10^{-6} A/m to 1 x 10^{-4} A/m that were considered reasonable values for carbonate sediments and thus regarded as uncontaminated or only slightly contaminated. Discrete specimens taken from the inner part of the cores showed similar NRM intensity values corroborating the hypothesis that contamination was limited to the outer part of the cores.

Based on these remarks, box specimens for the shore-based analysis were collected from the inner part of the core in Site U1467 and were measured using a 2G-enterprise DC-SQUID magnetometers at the CIMaN-ALP laboratory (Cuneo, Italy).~~.~~ Samples were progressively demagnetized in alternating field (AF) up to the maximum field of 100 mT according to a standard paleomagnetic procedure.

The directional components of the natural magnetization were calculated using the method of the principal component analysis (Kirschvink, 1980) and the PuffinPlot software (Lurcock and Wilson, 2012).~~).~~ The quality of the measurements and the line fitting was checked by visual inspection of the orthogonal vector plots and was quantified using the maximum angular deviation (MAD).

The AF demagnetization technique was effective in demagnetizing the NRM testifying that low-coercivity minerals are the main carriers of the NRM. Vector plots generally show a small viscous overprint removed in fields smaller than 20 mT, while the remaining part of the NRM is demagnetized in the field interval from 20 mT to 100 mT. The component isolated within this coercivity interval was used to calculate the characteristic remanent magnetization (ChRM) when sufficiently linear and well defined. However, the success rate in recovering reliable paleomagnetic directions was generally low and many specimens were discarded because they did not yield ~~to~~ results with acceptable quality. In specimens that gave acceptable results, on average, about 20% of the NRM was removed after AF demagnetization at 20 mT, and ca. 95% of the NRM was removed at field of 60 mT. Moreover, the NRM median destructive field of acceptable specimens (Fig. 2b) has a modal value of 10 mT. The percentage of NRM removed at 60 mT and the values of median destructive field corroborate the results of IRM acquisition suggesting that stable NRM is carried by pseudo-single domain magnetite. In acceptable specimens~~In these specimens~~, the NRM intensity has an average value of~~averaged~~ ca. 2.1x10^{-4} A/m, the average value of MAD obtained from the vector analysis of these specimens was 8.9°. About 10% of specimens have MAD values between 15° and 20°, which although large, are~~have been~~ considered acceptable~~ anyway~~; most of these specimens are located in the upper part of the investigated interval, between 100 and 180 m depth, or at polarity transitions.~~150 mcd.~~ Representative orthogonal vector plots for Site U1467 are illustrated in Figure 3.

The azimuthal orientation of cores was essential for interpretation of magnetic polarity because the paleomagnetic inclinations of equatorial localities, such as Site U1467 during the Miocene, are very close to zero for both normal and reversed~~reversal~~ polarities; hence the geomagnetic polarities are indistinguishable if based only on inclination data. APC cores collected from Site U1467 were oriented using the "tensor tool" that provided a good first-order orientation. The average~~averaged~~ declinations from paleomagnetic measurements showed ~~indeed~~ significant departures~~departure~~ from~~ the~~ North and discrepancies between cores, suggesting that orientation errors of the tensor tool can be as large as ±30°. However, although large, these errors did not compromise the polarity of ChRM and there was~~were~~ no ambiguity in establishing the magnetic polarity. We did not attempt to remove orientation errors by adjusting the magnetic declination to a mean direction even if this resulted in a reduced precision of the latitude of the virtual geomagnetic pole (VGP).

3.3. Anisotropy of isothermal remanent magnetization

In agreement with shipboard measurements, the magnetic susceptibility of box-samples shows~~has shown~~ negative (diamagnetic) susceptibility, evidence of the dominating diamagnetic matrix of $CaCO_3$ on the ferrimagnetic component. The very weak ~~and negative (~~diamagnetic~~) magnetic~~ susceptibility of the carbonate sediments recovered in Site U1467 (Betzler et al., 2017) limits~~compromises~~ the possibility of using~~to use~~ the anisotropy of magnetic susceptibility to investigate the orientation pattern of the magnetic particles. Therefore, we resorted to using ~~resourced to the anisotropy of isothermal remanent magnetization (~~AIRM which~~) that~~ can be measured precisely even in these weakly magnetic sediments.

AIRM measurements were performed in a subset of 75 specimens taken from Core 13 to Core 26 of Hole U1467A.~~.~~ To compute the AIRM an isothermal remanent magnetization induced with a field of 20 mT was measured and then AF demagnetized, repeating this procedure along 6 different axes. Each axis was measured twice along opposite directions for a total of 12 AIRM measurements in each specimen~~directions~~ (e.g., Stephenson et al., 1986; Jackson, 1991; Potter, 2004).~~) for a total of 12 AIRM measurements in each specimen.~~ The intensity of isothermal magnetization was measured with a JR-6 spinner magnetometer and the specimens were demagnetized after each measurement using a tumbling 2G AF-demagnetizer at a maximum field of 80 mT, before inducing the magnetization in the next direction. The anisotropy tensor and~~,~~ the directions of the principal IRM axis I_i ~~magnetic lineation~~ (i.e., the eigenvectors~~the direction of the main eigenvector I_{max} of the anisotropy tensor) and the foliation plane (i.e., the plane orthogonal to smaller eigenvector I_{min}~~ of the AIRM~~anisotropy~~ tensor) were computed from the remanent magnetization using the AGICO software Anisoft42. The AIRM is therefore represented as a triaxial ellipsoid, whose principal axes correspond to the directions of maximum, intermediate and minimum IRM ($I_1 < I_2 < I_3$). The anisotropy ellipsoid was described using the corrected anisotropy degree (P’) and the shape parameter (T) computed according to Jelinek (1981)

$$T = (2n_1 - n_2 - n_3)/(n_1 - n_3)$$
$$P' = \sqrt{exp\ 2\ (a_1^2 + a_2^2 + a_3^2)}$$

where $n_i = \ln I_i$, $a_i = \ln\left(\frac{I_i}{I'_m}\right)$ and $I'_m = \sqrt[3]{I_1 I_2 I_3}$ with $i = 1,2,3$ and are shown in Figure 4.

The direction of the largest axis of the anisotropy tensor I_1 represents the magnetic lineation (the preferred orientation of elongated magnetic particles), and the foliation plane is the plane that contains the I_1 and I_2 directions, hence is orthogonal to the direction of the smallest axis of the anisotropy tensor I_3.

4. Results and discussion

4.1. Magnetostratigraphy

Declination, inclinations of ChRM and the resulting VGP latitude of Site U1467 are shown in Figure 5~~4~~ plotted versus depth m CSF-A~~mcd~~, together with the available biostratigraphic events from shipboard analysis (Betzler et al., 2017). The comparison of measured levels ~~Data quality~~ and ~~success rate are best below 150 mcd and it is only~~ acceptable samples~~in the upper 50 m of the measured interval. The density of data points~~ in Figure 5 indicates~~4 is indicative of~~ the low success rate ~~obtained~~ in finding reliable directions of the ChRM.~~, which was generally low.~~ Sometimes, ~~as~~ for instance in specimens taken from Hole U1467C, we could not obtain~~get~~ any acceptable results~~result~~. In general in the upper part of the Site above 110 m~~mcd~~, which comprises~~is comprised in~~ the sedimentological Unit I, the paleomagnetic data yielded poor results probably related to the coarser granulometry of the unlithified wackestone sediments. At depths~~depth comprised~~ between 100 m and 290 m~~mcd~~, the quality of the data was sufficient~~sufficiently good~~ to obtain a reliable record of polarity reversal, although with ~~a~~ variable quality.

In the interval with good data quality (i.e., the central part of the record with smaller MAD),~~,~~ the ChRM inclinations are practically indistinguishable from zero, regardless of the ~~actual~~ polarity, except for transitional directions corresponding to the time elapsed during the reversal of the geomagnetic field. Averaged paleomagnetic directions (Table 1) indicate an~~2) indicates a nearly~~ equatorial paleolatitude $\lambda = 0.8°$ ($\lambda^{+}_{95} = 4.4°$; $\lambda^{-}_{95} = -2.8°$) of Site U1467 during the early~~Lower~~ Pliocene within the precision of the paleomagnetic data~~, (colatitude error $dp_{95} = 3.6°$),~~ which is in agreement~~good accordance~~ with the paleogeographic reconstructions of Besse and Courtillot (2002) and Torsvik et al. (2012).

The record of polarity reversals identifies~~record has identified~~ 6 normal and 6 reversed magnetic polarity zones that, based on the biostratigraphic framework, have been interpreted as Chrons C2An.2n to C3n.4r (Fig. 6~~5~~) (Gradstein et al., 2012). This~~It has to be noticed that this~~ interpretation is manly based on the ~~only~~ 4 biostratigraphic events available in the studied section and located in the upper part of the record; however~~. Moreover~~, there is some uncertainty ~~uncertainties~~ even in the biostratigraphic data since the dates based on Last Occurrence~~lower appearance~~ of foraminifera (*Dentoglobigerina altispira* and *Globorotalia margaritae*) show a relatively large discrepancy with that of calcareous nannofossil~~nannoplanckton~~ events (LO *Sphenolithus abies* and LO *Reticulofenestra pseudoumbilicus*). Even though the~~The~~ few available biostratigraphic markers ~~available and their uncertainty~~ leave some room in interpreting which magnetochrons correspond to the measured polarity reversals, we~~. We~~ believe that our interpretation (Fig. 6)~~shown in Figure 5~~ is the best compromise between a reduced variability of the sedimentation rate and the available biostratigraphic framework.~~, nonetheless, we realize that this interpretation could change if major modification were made to the biostratigraphy data.~~ Within these limitations, the magnetic stratigraphy of Site U1467 provides~~provide~~ a robust age constraint~~constrains~~ in a section where~~were~~ biostratigraphic records are~~record is~~ unavailable.

In our interpretation the age of the studied section spans ca. from 5.3 Ma ~~Myr ago~~ to 3.1 Ma~~Myr ago~~, as reported in detail~~details~~ in Table 2~~1~~.

4.2. Anisotropy of the IRM

According to a number of studies (e.~~,~~g., ~~Lüdmann et al., 2013;~~ Betzler et al., 2009, 2016b~~2016~~, 2018 and references~~reference~~ therein) bottom currents in the~~The~~ Maldives platform are considered wind-driven and assumed to be ~~are considered~~ a direct consequence of -Asian monsoon. At equatorial latitudes, the link between surface wind and bottom currents extends to a depth of several hundred meters either through Ekman transport or as an undercurrent system and can be seen with modern observations. The present day equatorial Indian Ocean is characterized by seasonally reversing surface currents, known as Wyrtki Jets, driven by zonal winds. Beneath the surface, to a depth of several hundred meters, the flow of the equatorial undercurrent and the equatorial intermediate current has been observed (e.g., Knox, 1976; Reppin et al., 1999; Schott and McCreary, 2001; Iskandar et al., 2009; Nyadjro et al., 2015). In contrast to other oceans, the Indian Ocean equatorial undercurrent is transient and strongly dependent on winds and pressure gradient variations. Both eastward and westward flows of sub-surface currents have been observed, although modeling studies based on the present day suggest that eastward undercurrents are more likely to occur than westward ones (Schott and McCreary, 2001). Since sub-surface currents develop as consequences of surface wind it is reasonable to assume that stronger surface winds will increase the strength of the undercurrent, and following~~Following~~ this argument~~line~~, we interpret bottom current ~~paleo-direction and~~ strength as proxy of the paleo-monsoon.

Magnetic methods are ~~In this case the magnetic method is~~ particularly useful when~~failing~~ other quick methods for determining paleo flow~~paleoflow~~ from sediment beds such as macroscopic paleocurrent indicators (e.g., cross-stratification and sole marks) are lacking.~~).~~ In standard analysis of magnetic grain shape fabric, AIRM is considered to be a proxy for the preferred alignment of elongated natural magnetic particles attained in the final stages of transport, with I_1~~I_{max}~~ and I_3~~I_{min}~~ representing preferred orientations of the longest and shortest grain axes, respectively (e.g., Hamilton and Rees, 1970, Taira and Scholle, 1979; Novak, 2014, Felletti 2016). The method assumes implicitly that the uniaxial shape-anisotropy of magnetic particles dominates triaxial magnetocrystalline anisotropy, as expected~~ which is a very reasonable assumption~~ for elongated~~Site U1467 since~~ magnetite particles (e.g., Tauxe, 2002).~~is the main magnetic mineral.~~

According to theoretical, experimental and field-based fabric studies, two main anisotropic fabric patterns are found (e.g., Harms et al., 1982; Baas et al., 2007): (i) flow-aligned fabric; and (ii) flow-transverse fabric. In flow-aligned fabric the I_1~~I_{max}~~ axes are oriented parallel to the mean flow direction, while in a flow-transverse fabric~~,~~ the I_1~~I_{max}~~ axes are oriented perpendicular to the flow direction. In turbulent flows, grains settling from suspension tend to orient with their I_1~~I_{max}~~ axes parallel to the flow direction and imbricated upstream (Rusnak, 1957; Allen, 1984). This flow-aligned orientation can be changed into a more stable flow-transverse orientation when the flow becomes strong enough to lift grains and roll them over the surface (e.g. Schwarzacher, 1963; Johansson, 1964; Hendry, 1976, Harms et al., 1982). In both cases the *foliation* planes ~~(i.e., the planes perpendicular to the I_{min} axes)~~ can be imbricated dipping upstream (Harms et al., 1982) and the comparison of their orientation with I_1~~I_{max}~~ axes can be used to recognize the flow-aligned and flow-transverse fabrics.

Deviations from the flow-aligned or the flow-transverse fabrics can occur for a number of reasons ~~(e.g., Baas et al., 2007 and references therein~~which include~~) among which~~ spatial changes in current direction, bed surface irregularities, incomplete reorientation of a rolling fabric into a flow-aligned fabric or vice versa, changes in bed roughness and post-depositional modification by bioturbation or soft-sediment deformation ~~.~~(e.g., Baas et al., 2007 and references therein).

We recognise the pattern of each specimen~~In Site U1467, we found that the AIRM is significantly large to produce a coherent pattern of orientations only in the upper part on the analysed interval (Fig. 6). The degree of anisotropy (P' parameter) shows a sudden increase from very low values (mean 1.055±0.03) to larger values (mean 1.22± 0.17) in the upper ca. 168±2 mcd of Site U1467 corresponding to the age of about 4.2 Myr ago in our age model. In the upper part of Site U1467 the directions of the elongation axis I_{max} have a mean direction of 134/00. Foliation planes are imbricated toward NE and SW (Fig. 7)~~ by comparing the~~an~~

average angle (θ) between theof about 34° (a_{95} = 9.4). The averaged direction of the magnetic lineation I_1 and that of the foliation plunge. If $\theta < 35°$ the pattern is flow-alignedplanes of 137° N (angular dispersion 11°) and the flow is taken equal to declination of the I_1elongation axis in the directionindicate a transverse pattern of the foliation imbrication; if $\theta \geq 55°$ the pattern is flow-transverse and the flow is the declination of I_1 – 90° in theAIRM with a mean flow direction of the foliation imbrication. The intermediate case ($35° < \theta \leq 55°$) is handled by taking directly the imbrication orthogonal to both axis. According to this observation the direction of the foliation plane as the flow direction.

In Site U1467, we found that the AIRM is large enough to produce a well-defined pattern of orientations only if the degree of anisotropy P' ≥ 1.1, which mostly comprises specimens with flow-transverse pattern and located in the upper part on the sediment column. Current directions, foliation planes and I_1 directions are shown in bottom Figure 7 in separated sets for P' ≥ 1.1 and P' < 1.1 . In the set with P' ≥ 1.1, the current directions fall into two distinct groups with nearly opposite modal directions highlighted by the rose diagram (Fig. 7c). Foliation planes also have the opposite plunge and their direction is consistent with the current modes (Fig. 7 a). The mean current directions are computed as a mixture of 2 Von Mises distributions, which is necessary since we have two groups of directions and Von Mises distributions are unimodal. Calculations were performed using the R-package "movMF" (Hornik and Grün, 2014) and returned two independent distributions, the first with mean direction m=45.3° and concentration parameter k = 6.3, and a the second with mean direction m 227.4° and concentration parameter k = 2.2 (Fig. 7e). The current directions are nearly antipodal as expected for seasonally reversing monsoon-driven currents. In the set with P' < 1.1, the flow directions, the foliation planes and I_1 axis appear dispersed, probably because bottom currents were absent or too weak to produce a coherent directional pattern in elongated sediment particles (Fig. 7b and Fig. 7d). A Kuiper test for uniformity accepted the Null hypothesis at the 95% confidence level testifying that these directions do not have a preferential orientation. According to these observations stratigraphic intervals with larger P' indicate the presence of stronger bottom currents that flowflows alternatively toward NE and SW. The N-S components of the observed currents are interpreted as a deflection of equatorial zonal currents in the Inner Sea of the Maldives where bottom currents are forced to follow the sea floor morphology and the directions of the main channels. Inferred current directions are ca. NE and ca. SW and is virtually identical to thosethat of present-day bottom current data measured bybe acoustic Doppler profiler by Lüdmann et al. (2013).

The presence of bottom currents is not constant throughout the stratigraphic record. In fact the degree of anisotropy P’ is generally very small in the lower part of the stratigraphic column (mean 1.05±0.03) and shows larger values (mean 1.22± 0.17) in the upper part with a sudden increase at about 168±2 m CSF-A, which corresponds to the top of Chron C3n.1n and an age of about 4.2 Ma (Fig. 8). The increase of anisotropy in the upper ~~ca.~~ 168 m CSF-A~~mcd~~ is synchronous with a more gradual decrease of IRM intensity, which is indicative of a decreased concentration of magnetic minerals. The decrease of IRM intensity can be interpreted as a superimposed long-term trend with an acceleration starting at the depth of ~168 m CSF-A (Fig. 8b).~~mineral (Fig. 6). Changes in magnetic properties correspond to the depth of seismic reflector DS8, which marks the boundary of a sedimentary sequence within the drift deposits of the Maldives inner sea (Lüdmann et al., 2018).~~ No changes in the main lithological units were observed at this depth (Betzler et al., 2017), however the decreased concentration of magnetite ~~2017). The change of magnetic properties at about 168±2 mcd~~ is followed by deteriorated quality of the paleomagnetic measurements and decreased sedimentation rate in the upper part of Site U1467. From the sedimentological point of view, the decrease of IRM is ~~tentatively~~ interpreted as a consequence of changes in the sediment transport mechanism - controlled by wind driven currents- that transferred the sediments and the single-domain magnetite, possibly of biogenic origin, from the shallow platform to the deeper water of Site U1467 (Lüdmann et al., 2013). This process is modified by the increased monsoon strength starting at ~168 m CSF-A and the depocenter of drift deposits moving downstream. Regardless of~~Regardless~~ the reason for the IRM decrease, the increased anisotropy can be associated with~~to the~~ changes in sedimentation dynamics~~dynamic~~ that lead to ~~the~~ drift deposition and that has been related to the onset of strong modern monsoon system (Betzler et al., 2016b). ~~2016). Hence, we assume that stronger bottom currents, indicated by higher anisotropy parameter P’, corresponds to stronger monsoon.~~

Our results suggest that starting from the lower Pliocene (ca. 4.2 Myr ago) the monsoon-related bottom currents became strong~~stronger~~ enough to significantly increase the degree of anisotropy and create a mostly transverse pattern in the sediments with ~~significant~~ large AIRM. Increased~~Increase of~~ monsoon strength could qualitatively be explained with the onset of the intertropical convergence zones (ITCZ) to their present-day position. This implies ~~with~~ a southern shift of the ITCZ south of the Himalayas~~Himalaya~~ and an increase in the latitudinal separation of the summer and winter ITCZ that moved the winter ITCZ south of the~~The~~ Maldives (e.g., Allen and Armstrong, 2012 and references~~reference~~ therein). The Himalayas~~Himalaya~~ and Tibet have a~~are of~~ primary influences on atmospheric circulation patterns and hence climate of the region. For this reason the surface uplift history of the Himalayan-Tibetan orogen has been suggested to be closely linked to the development of the Asian monsoon (Clift et al., 2008) and in fact, Tibetan plateau and Himalayan uplift is considered necessary for the presence of the strong present day monsoon (Prell and Kutzbach, 1997).

During the late Cenozoic the regional uplift may have occurred in two stages, one beginning in the Late Miocene, which~~that has~~ probably led to the beginning of the drift deposition at 12.9 Ma (Betzler et al., 2016b),~~2016)~~ followed by a later Pliocene phase dated approximately from 5 to 2 Myr ago (Harrison et al, 1992; Zheng et al., 2000; An et al., 2001) that could have been recorded in ~~the~~ Site U1467 ~~record~~. Independent evidence supporting a coeval increase of monsoon intensity through enhanced precipitation, occurring at about 4 Ma~~Myr ago~~, is given by the magnetic susceptibility record from ODP site 758, (Prell and Kutzbach, 1997, An et al., 2001), which is interpreted as the sea-level-mediated fluvial transport from the Ganges and other river systems draining the southern side of the Himalaya-Tibet plateau. Moreover, Zheng et al., (2000) interpret the increase in sedimentation rate and change in depositional facies from redbeds to upward-coarsening conglomerate and debris-flow deposits at the foot of the Kunlun Mountains~~,~~ as evidence for the uplift of the north-western~~northwestern~~ Tibetan Plateau ~~began~~ between 3.5 and 4.5 Ma. The timing of increased current strength in the~~The~~ Maldives platform is compatible with the beginning of the Pliocene uplift stage, and in fact this could mark precisely the beginning of climatic influence of the Pliocene Himalayan uplift at 4.2 Ma~~Myr ago~~.

5. Conclusions

Paleomagnetic study of IODP Site U1467 provides~~provided~~ a magnetic stratigraphy that gives~~gave~~ an improved age model of the Pliocene portion of Site U1467 compensating for the scarcity of the biostratigraphic data in this time interval. This new age model can potentially be the basis for further astrochronological studies.

The analysis of the AIRM has shown evidence of bottom currents with alternating directions similar~~that correspond~~ to the present-day currents~~. originating from Asian monsoon.~~ We found that the strength of the bottom currents inferred from the AIRM-corrected anisotropy degree P' ~~parameter~~ increased suddenly at about 4.2 Myr ago. This is interpreted as~~, according to our age model. In~~ the formation~~stratigraphic record, the change in current strength corresponds to the depth~~ of stronger equatorial undercurrents as a consequence of~~seismic reflector DS8 (Lüdmann et al., 2018) and suggests that the~~ increased monsoon strength~~-related bottom currents had a direct effect on sediment transportation within The Maldives platform~~.

A number of studies relate the strength of Asian monsoon to the uplift of the HimalayasHimalaya~~Himalaya~~ and Tibetan plateau. We observe that the timing of the increase of bottom currents~~current~~ (4.2 Ma) coincides~~coincide~~ with the increase of fluvial transport to the Bay of Bengal and is compatible with the beginning of the Late Pliocene phase of Himalayan uplift, suggesting that is represents the Maldives record of the Late Pliocene uplift phase. In this case our age model gives~~give~~ a precise timing of this event.

Acknowledgments

The authors thank the crew of the JOIDES Resolution. Financial support for this research was provided by IODP-Italia and University of Urbino (DiSPeA) .~~.~~ Laboratory analyses were performed thanks to "Consorzio Interuniversitario di Magnetismo Naturale (CIMaN)". Two anonymous reviewers contributed to improve the manuscript.

Bibliography

1. An, Z., Kutzbach, J.E., Prell, W.L., Porter, S.C., 2001. Evolution of Asian monsoons and phased uplift of the Himalayan Tibetan plateau since Late Miocene times. Nature, 411, 62-66.
2. Allen, J.R.L., 1984. Sedimentary Structures: their Character and Physical Basis. Developments in Sedimentology, vol. 30A/B. Elsevier, Amsterdam. 593/663 pp.
3. Allen, M.B. and Armstrong, H.A., 2012. Reconciling the Intertropical Convergence Zone, Himalayan/Tibetan tectonics, and the onset of the Asian monsoon system, *Journal of Asian earth sciences.*, 44 . pp. 36-47.
4. Baas, J. H., Hailwood, E. A., McCaffrey, W. D., Kay, M. & Jones, R. 2007. Directional petrological characterisation~~charac- terisation~~ of deep-marine sandstones using grain fabric and permeability anisotropy: Methodologies, theory, application and suggestions for integration. Earth- Science Reviews, 82, 101–142.
5. Besse, J., and Courtillot, V. 2002. Apparent and true polar wander and the geometry of the geomagnetic field over the last 200 Myr, *J. Geophys. Res.*, 107(B11), 2300, doi: 10.1029/2000JB000050.
6. ~~Christian~~ Betzler C., ~~, Christian~~ Hübscher, C. ~~Sebastian~~ Lindhorst S. , ~~, John J.G.~~ Reijmer J.J.R., ~~, Miriam~~ Römer M, ~~, André W.~~ Droxler A.W. , ~~, Jörn~~ Fürstenau J. and ~~Thomas~~ Lüdmann T., ~~,~~ 2009, Monsoon-induced partial carbonate platform drowning (Maldives, Indian Ocean). Geology, 37(10): 867–870; doi: 10.1130/G25702A.1
7. Betzler, C., Fürstenau, J., Lüdmann, T., Hübscher, C., Lindhorst, S., Paul, A., Reijmer, J.J.G., and Droxler, A.W., 2013. Sea-level and ocean-current control on carbonate-platform growth, Maldives, Indian Ocean. *Basin Research*, 25(2):172–196.
8. Betzler, C.G., Eberli, G.P., Alvarez Zarikian, C.A., and the Expedition 359 Scientists, 2016. Expedition 359 Preliminary Report: Maldives Monsoon and Sea Level. International Ocean Discovery Program. http://dx.doi.org/10.14379/iodp.pr.359.2016
9. Betzler, C., G.P. Eberli, D. Kroon, J.D. Wright, P.K. Swart, B.N. Nath, C.A. Alvarez-Zarikian, et al. 2016(b). ~~.~~ The Abrupt Onset of the Modern South Asian Monsoon Winds. *Scientific Reports* 6. https://doi.org/10.1038/srep29838.
10. Betzler, C., Eberli, G.P., Alvarez Zarikian, C.A., Alonso-García, M., Bialik, O.M., Blättler, C.L., Guo, J.A., Haffen, S., Horozal, S., Inoue, M., Jovane, L., Kroon, D., Lanci, L., Laya, J.C., Ling Hui Mee, A., Lüdmann, T., Nakakuni, M., Nath, B.N., Niino, K., Petruny, L.M., Pratiwi,

S.D., Reijmer, J.J.G., Reolid, J., Slagle, A.L., Sloss, C.R., Su, X., Swart, P.K., Wright, J.D., Yao, Z., and Young, J.R., 2017. Site U1467. *In* Betzler, C., Eberli, G.P., Alvarez Zarikian, C.A., and the Expedition 359 Scientists, *Maldives Monsoon and Sea Level*. Proceedings of the International Ocean Discovery Program, 359: College Station, TX (International Ocean Discovery Program). http://dx.doi.org/10.14379/iodp.proc.359.105.2017

11. Betzler, C., G.P. Eberli, D. Kroon, J.D. Wright, P.K. Swart, B.N. Nath, C.A. Alvarez-Zarikian, et al. 2018. Refinement of Miocene sea level and monsoon events from the sedimentary archive of the Maldives (Indian Ocean). *Progress in Earth and Planetary Science* 5:5 doi10.1186/s40645-018-0165-x

12. Clift, P.D., Hodges, K.V., Heslop, D., Hannigan, R., Van Long, H., Calves, G., 2008. Correlation of Himalayan exhumation rates and Asian monsoon intensity. Nature Geoscience, 1, 875-880.

13. Cleveland, W. S. (1979). Robust locally weighted regression and smoothing scatterplots. Journal of the American Statistical Association, 74, 829–836. doi: 10.1080/01621459.1979.10481038.

14. Cleveland, W. S., Grosse E. and Shyu W. M. (1992) Local regression models. Chapter 8 of Statistical Models in S eds J.M. Chambers and T.J. Hastie, Wadsworth & Brooks/Cole.

~~13.~~15. Felletti, F., Dall'Olio, E. and Muttoni G., 2016. Determining Flow Directions in Turbidites: An Integrated Sedimentological and Magnetic Fabric Study of the Miocene Marnoso Arenacea Formation (Northern Apennines, Italy). *Sedimentary Geology*. https://doi.org/10.1016/j.sedgeo.2016.02.009.

~~14.~~16. Gradstein, F.~~Felix~~ M., ~~James G.~~ Ogg J.G.,~~;~~ Mark D. Schmitz MD.,~~;~~ and ~~Gabi M.~~ Ogg G.M.,~~;~~ 2012. The Geologic Time Scale 2012. The Geologic Time Scale 2012. https://doi.org/10.1016/C2011-1-08249-8.

~~15.~~17. Hamilton, N., Rees, A.I., 1970. The use of magnetic fabric in paleocurrent estimation. In: Runcorn, S.K. (Ed.), Palaeogeophy- sics. Academic Press, New York, pp. 445–464.

~~16.~~18. Harrison, T. M., Copeland, P., Kidd, W. S. F. and Yin, A., 1992. Raising Tibet. Science 255, 1663-1670.~~. (1992).~~

~~17.~~19. Harms, J.C., Southard, J.B., Walker, R.G., 1982. Structures and Sequences in Clastic Rocks. SEPM Short Course, vol. 9. 249 pp.

~~18.~~20. Hendry, H.E., 1976. The orientation of discoidal clasts in resedimented conglomerates, Cambro-Ordovician, Gaspé, eastern Quebec. Journal of Sedimentary Petrology 46, 48–55.

21. Hornik K., Grün B., 2014. movMF: AnRPackage for Fitting Mixtures of von Mises-FisherDistributions. Journal of Statistical Software,58(10), 1–31. URLhttp://www.jstatsoft.org/v58/i10/

22.

23. Iskandar, I., Y. Masumoto, and K. Mizuno (2009), Subsurface equatorial zonal current in the eastern Indian Ocean, J. Geophys. Res., 114, C06005, doi:10.1029/2008JC005188.

~~19.~~24. Jackson, M., 1991. Anisotropy of magnetic remanence: A brief review of mineralogical sources, physical origins, and geological applications, and comparison with susceptibility anisotropy. PAGEOPH, 136: 1-28. https://doi.org/10.1007/BF00878885

25. Jelinek, V. 1981. "Characterization of the Magnetic Fabric of Rocks." Tectonophysics, 79, T63-T67, https://doi.org/10.1016/0040-1951(81)90110-4.

~~20.~~26. Johansson, C.E., 1964. Orientation of pebbles in running water: a laboratory study. *Geografiska Annaler* 45A, 85–112.

~~21.~~27. Kirschvink J. L., 1980. The least-squares line and plane and the analysis of palaeomagnetic data, *Geophysical Journal International*, 62, 3, 699–718, https://doi.org/10.1111/j.1365-246X.1980.tb02601.x

28. Knox, R. A. (1976), On a long series of measurements of Indian Ocean equatorial currents near Addu Atoll, Deep Sea Res. Oceanogr. Abstr., 23, 211–221.

29. Lurcock, P. C. and G. S. Wilson (2012), PuffinPlot: A versatile, user-friendly program for paleomagnetic analysis, Geochemistry, Geophysics, Geosystems, 13, Q06Z45, doi:10.1029/2012GC004098.

~~22.~~30. Lüdmann, T., Kalvelage, C., Betzler, C., Fürstenau, J., and Hübscher, C., 2013. The Maldives, a giant isolated carbonate platform dominated by bottom currents. *Marine and Petroleum Geology*, 43:326–340.

~~23.~~31. Lüdmann T., C. Betzler, G.P. Eberli, J. Reolid, J.J.G. Reijmer, C.R. Sloss, O.M. Bialik, C.A. Alvarez-Zarikian, M. Alonso-García, C.L. Blättler, J. A. Guo, S. Haffen, S. Horozal, M. Inoue, L. Jovane, D. Kroon, L. Lanci, J.C. Laya, A.LH. Mee, M. Nakakuni, B.N. Nath, K. Niino, L.M. Petruny, S.D. Pratiwi, A.L. Slagle, X. Su, P.K. Swart, J.D. Wright, Z. Yao, J.R. Young, 2018. Carbonate Delta Drift: A New Sediment Drift Type. Marine, Geology 401.

https://doi.org/10.1016/j.margeo.2018.04.011

32. Nyadjro, E. S., and M. J. McPhaden (2014), Variability of zonal currents in the eastern equatorial Indian Ocean on seasonal to interannual time scales, J. Geophys. Res. Oceans, 119, 7969–7986, doi:10.1002/2014JC010380.

~~24.~~33. Novak, B., Housen, B., Kitamura, Y., Kanamatsu, T., and Kawamura, K., 2014. Magnetic Fabric Analyses as a Method for Determining Sediment Transport and Deposition in Deep Sea Sediments. Marine Geology. https://doi.org/http://dx.doi.org/10.1016/j.margeo.2013.12.001.

~~25.~~34. Potter, D. K., 2004. A Comparison of Anisotropy of Magnetic Remanence Methods -- a User's Guide for Application to Palaeomagnetism and Magnetic Fabric Studies. In Geological Society, London, Special Publications. https://doi.org/10.1144/GSL.SP.2004.238.01.03.

~~26.~~35. Prell, W.L., and Kutzbach, J.E., 1992. Sensitivity of the Indian monsoon to forcing parameters and implications for its evolution. Nature, 360:647-652.

~~27.~~36. Prell, W.L., and Kutzbach, J.E., 1997. The impact of Tibet-Himalayan elevation on the sensitivity of the monsoon climate system to changes in solar radiation. In Ruddiman, W.F. (Ed.), Tectonic Uplift and Climate Change: New York (Plenum), 172-203.

~~28.~~37. Rea, D.K., 1992. Delivery of Himalayan sediment to the northern Indian Ocean and its relation to global climate, sea level, uplift, and seawater strontium. In: Duncan, R.A., Rea, D.K., Kidd, R.B., von Rad, U., Weissel, J.K. (Eds.), Synthesis of Results from Scientific Drilling in the Indian Ocean. Geophysical Monograph, vol. 70. Am. Geophys. Union, Washington DC, pp. 387–402.

38. Reppin, J., F. A. Schott, J. Fischer, and D. Quadfasel (1999), Equatorial currents and transports in the upper central Indian Ocean: Annual cycle and interannual variability, J. Geophys. Res., 104, 15,495–15,514.

~~29.~~39. Rusnak, G.A., 1957. The orientation of sand grains under conditions of "unidirectional" fluid flow: 1. Theory and experiment. Journal of Geology 65, 384–409.

40. Schott, F., and J. P. McCreary (2001), The monsoon circulation of the Indian Ocean, Prog. Oceanogr., 51, 1–123.

~~30.~~41. Schwarzacher, W., 1963. Orientation of crinoids by current action. Journal of Sedimentary Petrology 33, 580–586.

31.42. Stephenson, A., Sadikun, S., Potter, D.K., 1986. A theoretical and experimental comparison of the anisotropy of magnetic susceptibility and remanence in rocks and minerals. Geophys. J. R. astr. Soc., 84: 185-200.

32.43. Taira, A. and Peter Scholle, A., 1979. Origin of Bimodal Sands in Some Modern Environments. Journal of Sedimentary Research. https://doi.org/10.1306/212F7847-2B24-11D7-8648000102C1865D.https://doi.org/10.1306/212F7847-2B24-11D7-8648000102C1865D.

44. Tauxe, L., 2002. Paleomagnetic Principles and Practice. Modern Approaches in Geophysics. Vol. 17. New York: Springer.

33.45. Torsvik T.H., R. Van der Voo, U. Preeden, C. Mac Niocaill, B. Steinberger, P.V. Doubrovine, D.J.J. van Hinsbergen, M. Domeier, C. Gaina, E. Tohver, J.G. Meert, P.J.A. McCausland, L.R.M. Cocks, 2012. Phanerozoic polar wander, palaeogeography and dynamics, Earth-Science Reviews, 114, 325-368.

34.46. Wunsch, M. , Betzler, C. , Lindhorst, S. , Lüdmann, T. , Eberli, G. P. and Della Porta, G., 2017. Sedimentary dynamics along carbonate slopes (Bahamas archipelago). Sedimentology, 64: 631-657. doi:10.1111/sed.12317

35.47. Zheng, H., C. McAulay Powell, Z. An, J. Zhou, and G. Dong. 2000. Pliocene Uplift of the Northern Tibetan Plateau. Geology. https://doi.org/10.1130/0091-7613(2000)28<715:PUOTNT>2.0.CO;2.

Captions

Figure 1

Location map of IODP Site U1467.

Figure 2

Acquisition of isothermal remanent magnetization of representative samples from the investigated site (A) and the estimate of the density distribution of median destructive field of the natural remanent magnetization (B). Isothermal remanent magnetization acquisition shows that all~~. All measured~~ samples are saturated at fields higher than~~above~~ 100-150 mT indicating ~~that~~ the presence of~~only magnetic mineral has~~ low ~~-~~coercivity minerals. The low~~.~~ ~~Low~~ coercivity rules~~rule~~ out the presence of relevant amounts~~amount~~ of hematite or diagenetic iron-sulphides and suggests that magnetite (or maghemite) is the main magnetic mineral in the sediments. The histogram and the density distribution of the median destructive field has a mode of about 10 mT confirming that the natural remanent magnetization is carried by low-coercivity minerals.

Figure 3

Representative examples of vector plots of alternating field demagnetization of natural remanent magnetization.~~NRM.~~ Stepwise demagnetization of natural remanent magnetization~~NRM~~ of sediments from Site U1467 shows generally a very small overprint, which is removed at a maximum field of 10-20 mT, followed by a linear path toward the origin that is~~was~~ interpreted as the characteristic remanent magnetization.~~ChRM.~~ Blue segments represent the direction of the characteristic remanent magnetization~~ChRM~~ computed as the best-fit line of the selected demagnetization steps (shown in red).

Figure 4

Jelinek plot (Jelinek, 1981) illustrating the shape of anisotropy tensor (T) and corrected degree of anisotropy (P’). Symbol size is proportional to the intensity of isothermal remanent magnetization.

Figure 5~~4~~

ChRM directions (Declination and Inclination) , maximum angular deviation and virtual geomagnetic pole latitude plotted against core depth (m CFS-A).~~.~~ The latitude of the virtual geomagnetic pole is~~(VGP latitude) in~~ computed from the declination and inclination in~~on~~ order to better interpret the geomagnetic polarities, which are reported in the left column as black and white intervals for normal and reversed polarity, respectively. The horizontal dashed lines indicate cores breaks and the small symbols in the left side of the VGP Latitude panel indicates the measured levels.~~.~~ The biostratigraphic events, core photographs and sedimentary units from Betzler et al. (2017) are also reported.

Notice that the paleomagnetic inclinations are not significantly different from zero except for transitional directions, indicating an equatorial paleo-latitude of the site.

Figure 6~~5~~

Paleomagnetic interpretation and age model of the studied portion of Site U1467. Shipboard biostratigraphic events are reported to provide the general age frame. The reversal polarity sequence, N1 to N6, from Site U1467 is shown in the right-vertical axis. The~~, the~~ open circles connected by the red line represent the correlation of this polarity reversal sequence to the reference geomagnetic polarity scale on the horizontal upper axis.~~, according to our interpretation.~~

Figure 7

A and B) Equal area projection of the main anisotropy axis I_1 and foliation planes for the specimens sets with P’ ≥ 1.1 and P’ < 1.1, respectively. I_1 axis are shown in different colours depending on their flow pattern. The set with P’ ≥ 1.1, mostly taken above 168±2 m CSF-A, shows foliation planes imbricated along the current direction, in this case imbrications approximately toward NE and SW indicates currents flowing alternatively in these opposite directions. C and D) Current directions shows in the circular plots (dots) together with their rose diagram. The set with P’ ≥ 1.1 shows two distinct modal values while the set with P’ < 1.1 have uniformly distributed directions. E) Von Mises distributions and mean values (red arrows) for the set of current directions with P’ ≥ 1.1.

Figure 8~~6~~

Summary of anisotropy of isothermal remanent magnetization~~AIRM~~ data versus depth. ~~The~~ P’ ~~parameter~~ indicates the corrected anisotropy degree ~~of anisotropy~~, the shape parameter T is illustrated with a colour code. The IRM is indicative of concentration of magnetic minerals.

Data have been smoothed using the locally weighted regression method (Cleveland 1979, Cleveland et al., 1992) to illustrate the main trend. The 95% confidence level is shown by the grey band. The reversal polarity column provides a time frame and ties the age of the green~~grey~~ band marking the shift toward higher anisotropy and lower IRM intensity to the top of chron C3n.1n.

~~Figure 7~~

~~Equal area projection of the I_{min} anisotropy axis and foliation planes restricted to samples taken above 168±2 mcd, which correspond to the Site section with higher P'. Foliation planes are imbricated along the current direction, in this case imbrications approximately toward NE and SW indicates currents flowing alternatively in these opposite directions. The planes show mostly imbrications with moderate inclinations; planes in red are somewhat anomalous because of the high inclination.~~

Highlights

- Magneto-stratigraphic age model of Pliocene sediments from Site U1467
- Record of bottom currents from anisotropy of isothermal remanent magnetization
- Monsoon-related bottom currents increase at about 4.2 Ma
- Bottom currents increase is coeval with Late Pliocene phase of Himalayan uplift

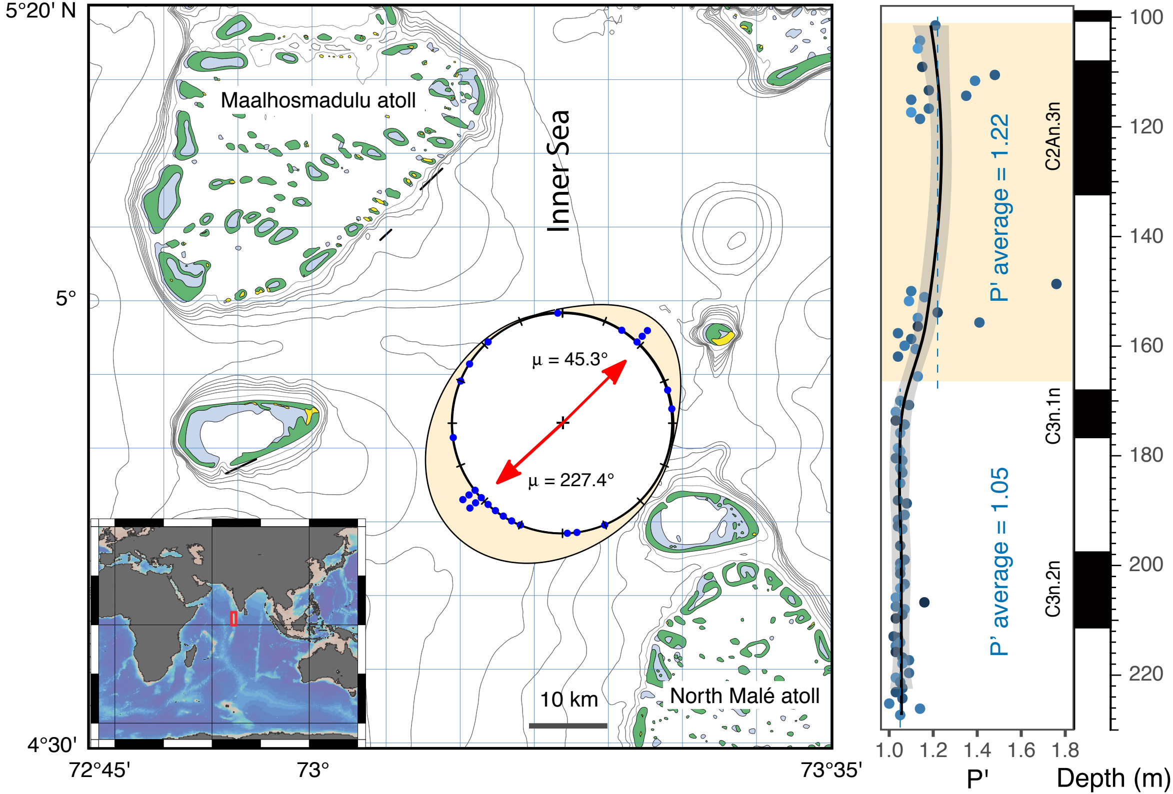

5°20' N
5°
4°30'
72°45'
73°
73°35'
Maalhosmadulu atoll
Inner Sea
North Malé atoll
10 km
μ = 45.3°
μ = 227.4°
P' average = 1.22
P' average = 1.05
C2An.3n
C3n.1n
C3n.2n
100
120
140
160
180
200
220
1.0
1.2
1.4
1.6
1.8
P'
Depth (m)

Magnetic properties of early Pliocene sediments from IODP Site U1467 (Maldives platform) reveal changes in the monsoon system

Luca Lanci[1,2], Elena Zanella[2,3], Luigi Jovane[4], Simone Galeotti[1], Montserrat Alonso-García[5,6], Carlos A. Alvarez-Zarikian[7], Christian Betzler[8], Or M. Bialik[9], Clara L. Blättler[10], Gregor P. Eberli[11], Junhua Adam Guo[12], Sébastien Haffen[13], Senay Horozal[14], Mayuri Inoue[15], Dick Kroon[16], Juan Carlos Laya[17], Anna Ling Hui Mee[11], Thomas Lüdmann[8], Masatoshi Nakakuni[18], Nagender Nath Bejugam[19], Kaoru Niino[20], Loren M. Petruny[21], Santi D. Pratiwi[22], John J. G. Reijmer[23], Jesús Reolid[24], Angela L. Slagle[25], Craig R. Sloss[26], Xiang Su[27], Peter K. Swart[11], James D. Wright[28], Zhengquan Yao[29, 30], Jeremy R. Young[31]

1) Department of Pure and Applied Science, University of Urbino, Via S. Chiara 27, 61029 Urbino, Italy.
2) Alpine Laboratory of Paleomagnetism ALP - CIMaN, Via G.U. Massa 6, 12016 Peveragno, Italy
3) Department of Earth Sciences, University of Turin, Via Valperga Caluso 35, 10125 Turin, Italy
4) Instituto Oceanográfico da Universidade de São Paulo, Praça do Oceanográfico, 191, São Paulo, SP 05508-120, Brazil.
5) Divisão de Geologia e Georecursos Marinhos, Instituto Portugues do Mar e da Atmosfera (IPMA), Avenida de Brasilia 6, 1449-006 Lisbon, Portugal.
6) Centro de Ciencias do Mar (CCMAR), Universidade do Algarve, Faro, Portugal.
7) International Ocean Discovery Program, Texas A&M University, 1000 Discovery Drive, College Station, TX 77845, USA.
8) Institute for Geology, CEN, University of Hamburg, Bundesstrasse 55, 20146 Hamburg, Germany.
9) Dr. Moses Strauss Department of Marine Geosciences, The Leon H. Charney School of Marine Sciences, University of Haifa, 31905 Carmel, Israel.
10) Department of the Geophysical Sciences, University of Chicago, 5734 S. Ellis Ave., Chicago, IL 60637, USA.
11) Department of Marine Geosciences, Department of Marine Geosciences, Rosenstiel School of Marine and Atmospheric Science, University of Miami, Miami, FL 33149, USA.
12) Department of Geological Sciences, California State University Bakersfield, 9001 Stockdale Highway, Bakersfield, CA 93311, USA.
13) Physical Properties Specialist, Ecole Nationale Superieure de Geologie, Universite de Lorraine, 2 rue du Doyen Marcel Roubault, 54501 Vandoeuvre-les-Nancy, France.
14) Petroleum and Marine Research Division, Korea Institute of Geoscience and Mineral Resources (KIGAM), Gwahang-no 124, Yuseong-gu, Daejeon 305-350, Korea.
15) Graduate School of Natural Science and Technology, Okayama University, 3-1-1 Tsushima-naka, Okayama 700-8530, Japan.
16) Department of Geology and Geophysics, University of Edinburgh, Grant Institute, The King's Buildings, West Mains Road, Edinburgh EH9 3JW, UK.

17) Department of Geology and Geophysics, Texas A&M University, Mail Stop 3115, College Station, TX 77843-3115, USA.
18) Department of Environmental Engineering for Symbiosis, Soka University, 1-236 Tangi-cyo, Hachioji-shi, Tokyo 192-0003, Japan.
19) Geological Oceanography Division, CSIR-National Institute of Oceanography, Dona Paula, Goa 403004, India.
20) Graduate School of Science and Engineering, Yamagata University, 1-4-12 Kojirakawa-machi, Yamagata City 990-8560, Japan.
21) Environmental Science and Policy Department, George Mason University, David King Hall Rm 3005, MSN 5F2, 4400 University Drive, Fairfax, VA 22030-4444, USA.
22) Department of Geosciences, Geotechnology and Materials Engineering for Resources, Akita University, 1-1 Teagata-Gakuencho, Akita 010-8502, Japan.
23) College of Petroleum Engineering and Geosciences, King Fahd University of Petroleum and Minerals, Dhahran 31261, Saudi Arabia.
24) Departamento de Estratigrafía y Paleontología, Universidad de Granada, Avenida de La Fuente Nueva S/N, 18071, Granada, Spain.
25) Lamont-Doherty Earth Observatory, Columbia University, Borehole Bldg. 61 Route 9W, Palisades, NY 10964, USA.
26) Earth and Environmental Sciences, University of Technology Queensland, R-Block 317, 2 George Street, Brisbane, QLD 4001, Australia.
27) Key Laboratory of Marginal Sea Geology, South China Sea Institute of Oceanology, Chinese Academy of Sciences, 164 West Xingang Road, Guangzhou 510301, People's Republic of China.
28) Department of Geological Sciences, Rutgers, The State University of New Jersey, 610 Taylor Road, Piscataway, NJ 08854-8066, USA.
29) Department of Marine Geology, First Institute of Oceanography (FIO) State Oceanic Administration (SOA), #6 Xian Xia Ling Road, Qingdao 266061, Shandong Province, People's Republic of China.
30) Laboratory for Marine Geology, Qingdao National Laboratory for Marine Science and Technology, Qingdao, People's Republic of China.
31) Department of Earth Sciences, University College London, Gower Street, London WC1E 6BT, UK.

Abstract

We report a study of the magnetic stratigraphy and the anisotropy of isothermal remanent magnetization of Pliocene sediments from International Ocean Discovery Program (IODP) Site U1467 drilled in the Maldives platform (Indian Ocean) during Exp. 359. Magnetic stratigraphy gives a precise record of geomagnetic reversals of the early Pliocene from approximately 5.3 Ma to 3.1 Ma providing a detailed age model in an interval where the biostratigraphic record is scarce. We use the anisotropy of isothermal remanent magnetization (AIRM) to investigate the statistical orientation of fine magnetic particles and provide data on the strength and direction of bottom currents during the early Pliocene. The strength of bottom currents recorded by the AIRM, shows a prominent increase at the top of Chron C3n.1n (about 4.2 Ma), and the current direction (NE - SW) is consistent with that of modern instrumental measurements. Since bottom currents in the Maldives are driven by the monsoon, we speculate that the 4.2 Ma increase of bottom currents could mark the onset of the present-day setting, probably related to the coeval uplift phase of the Himalayan plateau.

Keywords: Paleomagnetism; Pliocene magnetic stratigraphy; Anisotropy of isothermal remanent magnetization; Currents strength; Monsoon

1. Introduction

Wind-induced currents are an important factor controlling the sedimentation in the Maldives archipelago where they regulate sediment transport from the atoll to the deeper part of the platform as well as the geometry of the sedimentary bodies (e.g., Betzler et al., 2009; Lüdmann et al., 2013; Betzler et al., 2016b). The onset of these current-driven drift deposits has been related to the increase of monsoon activity starting in the middle Miocene (Betzler et al., 2016b). In this paper we report results from paleo and rock-magnetic analyses from International Ocean Discovery Program (IODP) Site U1467 aiming to improve the Pliocene age model and investigate the variations of bottom current strength.

Site U1467 (4° 51.0155' N and 73° 17.0204' E) was drilled in the Inner Sea of the Maldives archipelago (Indian Ocean) during IODP Expedition 359 at a water depth of 487.4 m (Betzler et al., 2017) in a distal position compared to the platform margins and moats (Fig. 1). Site U1467 showed nearly horizontally layered seismic reflections of the so-called drift sequences (Betzler et al., 2013, Lüdmann et al., 2013; Wunsch et al., 2017) with no truncations and no indications of mass wasting from the adjacent platform margin. Shipboard analysis suggested that Site U1467 provided a complete and undisturbed succession of all drift sequences from the Late Miocene (Betzler et al., 2017) with good potential for paleoceanographic and paleoclimatic studies. In particular the drift succession, from mid-Miocene to recent, contains several sequences that are potentially related to fluctuations in the monsoon-driven current system. Dating these sequences can yield the ages of changes in the strength and direction of the currents.

The paleomagnetic analysis in this study provides the magnetostratigraphic age of the upper portion of Site U1467 that was sampled with advanced piston coring (APC), and uses the anisotropy of the isothermal remanent magnetization (AIRM) to investigate the statistical orientation of fine magnetic particles aiming to provide a sedimentological record of direction and strength of bottom currents.

Shipboard paleomagnetic measurements of Site U1467 (Betzler et al., 2016, Betzler et al., 2017) gave poor results because of a combination of two factors: (i) the very low concentration of magnetic minerals in carbonate platform sediments, which resulted in a very weak natural remanent magnetization (NRM) and (ii) a strong magnetic contamination of the cores due to metallic particles presumably originating from the drilling pipes. The contamination covered the original weak paleomagnetic signal of the sediment preventing any valuable measurements with the shipboard pass-through technique that measures half-cores. Measurements of individual 7 cm^3 box-samples, taken from the inner part of the core, performed aboard, did not show signs of significant contamination suggesting that it was restricted to the outer part of the cores. Unfortunately, the NRM of these specimens, ranging from ca. 1×10^{-5} A/m to 1×10^{-4} A/m, was too weak to be measured reliably using the JR-6 spinner magnetometer available on the Joides Resolution. However, the NRM of the supposedly uncontaminated box-samples is within the range of sensitivity of a DC-SQUIDS cryogenic magnetometer, and this provided the motivation to collect and measure 580 standard sediment specimens with the aim to obtain a reliable magnetic stratigraphy of Site U1467.

2. Material and sampling

Standard paleomagnetic specimens (Natsuhara-Giken sampling cubes, with a volume of 7 cm^3) were collected in the upper part of Site U1467 from core sections 359-U1467B-11H to 359-U1467B-34H and from 359-U1467C-10H to 359-U1467C-17H, corresponding to 84 m to 302 m core depth below sea floor (CSF-A), at the Gulf Coast Repository at Texas A&M University. Specimens were sampled only from azimuthally-oriented APC cores, since information on core orientation is essential for paleomagnetic studies at equatorial latitudes such as for Site U1467.

According to the shipboard sedimentology, the studied part of Site U1467 was divided into three main lithostratigraphic units (Betzler et al., 2017). The uppermost Unit I was recovered in the top 110 m CSF-A and consists of unlithified, foraminifer-rich wackestone to packstone with a predominance of very fine- to fine-grained wackestone. Unit II extends from ca. 110 m to 215 m CSF-A; it comprises late Pliocene sediments and is characterized by interlayered unlithified and partially lithified planktonic foraminifera–rich wackestone and mudstone with pteropods and particulate organic matter. Unit III, which extends from 215 m to 303 m CSF-A, consists of partially lithified very fine–grained mudstone to wackestone with a dominance of wackestone. The sediment contains abundant planktonic foraminifera; echinoid spines and sponge spicules are common while benthic foraminifera are rare. Microfossil preservation throughout Units III and most of Unit II was generally poor to moderate, and in particular the interval from ca. 150 m to 300 m yields no biostratigraphic ages. The interval chosen for paleomagnetic study was also intended to cover this interval with poor or absent biostratigraphy.

3. Paleomagnetic analysis

3.1. Isothermal remanent magnetization

Magnetic mineralogy was investigated by acquisition of isothermal remanent magnetization (IRM) in a set of pilot specimens. IRM was acquired in 12 stepwise increasing fields from 0.03 T to 1 T, induced using a ASC pulse magnetizer (Fig. 2a). Results indicate that all measured specimens are characterized by the presence of only low-coercivity magnetic minerals that saturate in fields between 100 mT and 250 mT. These coercivities are below the maximum coercivity of uniaxial magnetite (e.g. Tauxe , 2002) and suggest a rather homogeneous mineralogy made of ferromagnetic minerals such as magnetite (or maghemite) without any significant presence of diagenetic iron sulphides that can be distinguished from their higher coercivity (e.g., Tauxe, 2002).

The saturated isothermal remanent magnetization is relatively weak, as often found in carbonate sediments, because of the low concentration of ferrimagnetic minerals. It ranges from 1.0×10^{-3} to 3.7×10^{-2} A/m, suggesting a wide variability in the concentration of magnetic minerals.

3.2. Natural remanent magnetization

The pass-through shipboard measurements of the NRM showed a huge scope of values with intensity ranging from 5×10^{-6} A/m to 1×10^{-1} A/m along the same core and with a strong downcore decreasing trend (Betzler et al., 2017). This was interpreted as the consequence of steel contamination most likely originating from worn off drill pipes. The bottom part of each APC core, which were the least contaminated, exhibited NRM values ranging from ca. 5×10^{-6} A/m to 1×10^{-4} A/m that were considered reasonable values for carbonate sediments and thus regarded as uncontaminated or only slightly contaminated. Discrete specimens taken from the inner part of the cores showed similar NRM intensity values corroborating the hypothesis that contamination was limited to the outer part of the cores.

Based on these remarks, box specimens for the shore-based analysis were collected from the inner part of the core in Site U1467 and were measured using a 2G-enterprise DC-SQUID magnetometers at the CIMaN-ALP laboratory (Cuneo, Italy). Samples were progressively demagnetized in alternating field (AF) up to the maximum field of 100 mT according to a standard paleomagnetic procedure.

The directional components of the natural magnetization were calculated using the method of the principal component analysis (Kirschvink, 1980) and the PuffinPlot software (Lurcock and Wilson, 2012). The quality of the measurements and the line fitting was checked by visual inspection of the orthogonal vector plots and was quantified using the maximum angular deviation (MAD).

The AF demagnetization technique was effective in demagnetizing the NRM testifying that low-coercivity minerals are the main carriers of the NRM. Vector plots generally show a small viscous overprint removed in fields smaller than 20 mT, while the remaining part of the NRM is demagnetized in the field interval from 20 mT to 100 mT. The component isolated within this coercivity interval was used to calculate the characteristic remanent magnetization (ChRM) when sufficiently linear and well defined. However, the success rate in recovering reliable paleomagnetic directions was generally low and many specimens were discarded because they did not yield results with acceptable quality. In specimens that gave acceptable results, on average, about 20% of the NRM was removed after AF demagnetization at 20 mT, and ca. 95% of the NRM was removed at field of 60 mT. Moreover, the NRM median destructive field of acceptable specimens (Fig. 2b) has a modal value of 10 mT. The percentage of NRM removed at 60 mT and the values of median destructive field corroborate the results of IRM acquisition suggesting that stable NRM is carried by pseudo-single domain magnetite. In acceptable specimens, the NRM intensity has an average value of ca. 2.1×10^{-4} A/m, the average value of MAD obtained from the vector analysis of these specimens was 8.9°. About 10% of specimens have MAD values between 15° and 20°, which although large, are considered acceptable; most of these specimens are located in the upper part of the investigated interval, between 100 and 180 m depth, or at polarity transitions. Representative orthogonal vector plots for Site U1467 are illustrated in Figure 3.

The azimuthal orientation of cores was essential for interpretation of magnetic polarity because the paleomagnetic inclinations of equatorial localities, such as Site U1467 during the Miocene, are very close to zero for both normal and reversed polarities; hence the geomagnetic polarities are indistinguishable if based only on inclination data. APC cores collected from Site U1467 were oriented using the "tensor tool" that provided a good first-order orientation. The average declinations from paleomagnetic measurements showed significant departures from North and discrepancies between cores, suggesting that orientation errors of the tensor tool can be as large as ±30°. However, although large, these errors did not compromise the polarity of ChRM and there was no ambiguity in establishing the magnetic polarity. We did not attempt to remove orientation errors by adjusting the magnetic declination to a mean direction even if this resulted in a reduced precision of the latitude of the virtual geomagnetic pole (VGP).

3.3. Anisotropy of isothermal remanent magnetization

In agreement with shipboard measurements, the magnetic susceptibility of box-samples shows negative (diamagnetic) susceptibility, evidence of the dominating diamagnetic matrix of $CaCO_3$ on the ferrimagnetic component. The very weak diamagnetic susceptibility of the carbonate sediments recovered in Site U1467 (Betzler et al., 2017) limits the possibility of using the anisotropy of magnetic susceptibility to investigate the orientation pattern of the magnetic particles. Therefore, we resorted to using AIRM which can be measured precisely even in these weakly magnetic sediments.

AIRM measurements were performed in a subset of 75 specimens taken from Core 13 to Core 26 of Hole U1467A. To compute the AIRM an isothermal remanent magnetization induced with a field of 20 mT was measured and then AF demagnetized, repeating this procedure along 6 different axes. Each axis was measured twice along opposite directions for a total of 12 AIRM measurements in each specimen (e.g., Stephenson et al., 1986; Jackson, 1991; Potter, 2004). The intensity of isothermal magnetization was measured with a JR-6 spinner magnetometer and the specimens were demagnetized after each measurement using a tumbling 2G AF-demagnetizer at a maximum field of 80 mT, before inducing the magnetization in the next direction. The anisotropy tensor and the directions of the principal IRM axis I_i (i.e., the eigenvectors of the AIRM tensor) were computed from the remanent magnetization using the AGICO software Anisoft42. The AIRM is therefore represented as a triaxial ellipsoid, whose principal axes correspond to the directions of maximum, intermediate and minimum IRM ($I_1 < I_2 < I_3$). The anisotropy ellipsoid was described using the corrected anisotropy degree (P') and the shape parameter (T) computed according to Jelinek (1981)

$$T = (2n_1 - n_2 - n_3)/(n_1 - n_3)$$

$$P' = \sqrt{\exp 2\,({a_1}^2 + {a_2}^2 + {a_3}^2)}$$

where $n_i = \ln I_i$, $a_i = \ln\left(\frac{I_i}{I'_m}\right)$ and $I'_m = \sqrt[3]{I_1 I_2 I_3}$ with $i = 1,2,3$ and are shown in Figure 4.

The direction of the largest axis of the anisotropy tensor I_1 represents the magnetic lineation (the preferred orientation of elongated magnetic particles), and the foliation plane is the plane that contains the I_1 and I_2 directions, hence is orthogonal to the direction of the smallest axis of the anisotropy tensor I_3.

4. Results and discussion

4.1. Magnetostratigraphy

Declination, inclinations of ChRM and the resulting VGP latitude of Site U1467 are shown in Figure 5 plotted versus depth m CSF-A, together with the available biostratigraphic events from shipboard analysis (Betzler et al., 2017). The comparison of measured levels and acceptable samples in Figure 5 indicates the low success rate in finding reliable directions of the ChRM. Sometimes, for instance in specimens taken from Hole U1467C, we could not obtain any acceptable results. In general in the upper part of the Site above 110 m, which comprises the sedimentological Unit I, the paleomagnetic data yielded poor results probably related to the coarser granulometry of the unlithified wackestone sediments. At depths between 100 m and 290 m, the quality of the data was sufficient to obtain a reliable record of polarity reversal, although with variable quality.

In the interval with good data quality (i.e., the central part of the record with smaller MAD), the ChRM inclinations are practically indistinguishable from zero, regardless of the polarity, except for transitional directions corresponding to the time elapsed during the reversal of the geomagnetic field. Averaged paleomagnetic directions (Table 1) indicate an equatorial paleolatitude λ = 0.8° (λ^{+}_{95} = 4.4°; λ^{-}_{95} = -2.8°) of Site U1467 during the early Pliocene within the precision of the paleomagnetic data, which is in agreement with the paleogeographic reconstructions of Besse and Courtillot (2002) and Torsvik et al. (2012).

The record of polarity reversals identifies 6 normal and 6 reversed magnetic polarity zones that, based on the biostratigraphic framework, have been interpreted as Chrons C2An.2n to C3n.4r (Fig. 6) (Gradstein et al., 2012). This interpretation is manly based on the 4 biostratigraphic events available in the studied section and located in the upper part of the record; however, there is some uncertainty even in the biostratigraphic data since the dates based on Last Occurrence of foraminifera (*Dentoglobigerina altispira* and *Globorotalia margaritae*) show a relatively large discrepancy with that of calcareous nannofossil events (LO *Sphenolithus abies* and LO *Reticulofenestra pseudoumbilicus*). Even though the few available biostratigraphic markers leave some room in interpreting which magnetochrons correspond to the measured polarity reversals, we believe that our interpretation (Fig. 6) is the best compromise between a reduced variability of the sedimentation rate and the available biostratigraphic framework. Within these limitations, the magnetic stratigraphy of Site U1467 provides a robust age constraint in a section where biostratigraphic records are unavailable. In our interpretation the age of the studied section spans ca. from 5.3 Ma to 3.1 Ma, as reported in detail in Table 2.

4.2. Anisotropy of the IRM

According to a number of studies (e.g., Betzler et al., 2009, 2016b, 2018 and references therein) bottom currents in the Maldives platform are considered wind-driven and assumed to be a direct consequence of Asian monsoon. At equatorial latitudes, the link between surface wind and bottom currents extends to a depth of several hundred meters either through Ekman transport or as an undercurrent system and can be seen with modern observations. The present day equatorial Indian Ocean is characterized by seasonally reversing surface currents, known as Wyrtki Jets, driven by zonal winds. Beneath the surface, to a depth of several hundred meters, the flow of the equatorial undercurrent and the equatorial intermediate current has been observed (e.g., Knox, 1976; Reppin et al., 1999; Schott and McCreary, 2001; Iskandar et al., 2009; Nyadjro et al., 2015). In contrast to other oceans, the Indian Ocean equatorial undercurrent is transient and strongly dependent on winds and pressure gradient variations. Both eastward and westward flows of sub-surface currents have been observed, although modeling studies based on the present day suggest that eastward undercurrents are more likely to occur than westward ones (Schott and McCreary, 2001). Since sub-surface currents develop as consequences of surface wind it is reasonable to assume that stronger surface winds will increase the strength of the undercurrent, and following this argument, we interpret bottom current strength as proxy of the paleo-monsoon.

Magnetic methods are particularly useful when other quick methods for determining paleo flow from sediment beds such as macroscopic paleocurrent indicators (e.g., cross-stratification and sole marks) are lacking. In standard analysis of magnetic grain shape fabric, AIRM is considered to be a proxy for the preferred alignment of elongated natural magnetic particles attained in the final stages of transport, with I_1 and I_3 representing preferred orientations of the longest and shortest grain axes, respectively (e.g., Hamilton and Rees, 1970, Taira and Scholle, 1979; Novak, 2014, Felletti 2016). The method assumes implicitly that the uniaxial shape-anisotropy of magnetic particles dominates triaxial magnetocrystalline anisotropy, as expected for elongated magnetite particles (e.g., Tauxe, 2002).

According to theoretical, experimental and field-based fabric studies, two main anisotropic fabric patterns are found (e.g., Harms et al., 1982; Baas et al., 2007): (i) flow-aligned fabric; and (ii) flow-transverse fabric. In flow-aligned fabric the I_1 axes are oriented parallel to the mean flow direction, while in a flow-transverse fabric the I_1 axes are oriented perpendicular to the flow direction. In turbulent flows, grains settling from suspension tend to orient with their I_1 axes parallel to the flow direction and imbricated upstream (Rusnak, 1957; Allen, 1984). This flow-aligned orientation can be changed into a more stable flow-transverse orientation when the flow becomes strong enough to lift grains and roll them over the surface (e.g. Schwarzacher, 1963; Johansson, 1964; Hendry, 1976, Harms et al., 1982). In both cases the *foliation* planes can be imbricated dipping upstream (Harms et al., 1982) and the comparison of their orientation with I_1 axes can be used to recognize the flow-aligned and flow-transverse fabrics. Deviations from the flow-aligned or the flow-transverse fabrics can occur for a number of reasons which include spatial changes in current direction, bed surface irregularities, incomplete reorientation of a rolling fabric into a flow-aligned fabric or vice versa, changes in bed roughness and post-depositional modification by bioturbation or soft-sediment deformation (e.g., Baas et al., 2007 and references therein).

We recognise the pattern of each specimen by comparing the angle (θ) between the direction of the magnetic lineation I_1 and that of the foliation plunge. If $\theta < 35°$ the pattern is flow-aligned and the flow is taken equal to declination of the I_1 axis in the direction of the foliation imbrication; if $\theta \geq 55°$ the pattern is flow-transverse and the flow is the declination of $I_1 - 90°$ in the direction of the foliation imbrication. The intermediate case ($35° < \theta \leq 55°$) is handled by taking directly the imbrication direction of the foliation plane as the flow direction.

In Site U1467, we found that the AIRM is large enough to produce a well-defined pattern of orientations only if the degree of anisotropy P' ≥ 1.1, which mostly comprises specimens with flow-transverse pattern and located in the upper part on the sediment column. Current directions, foliation planes and I_1 directions are shown in Figure 7 in separated sets for P' ≥ 1.1 and P' < 1.1 . In the set with P' ≥ 1.1, the current directions fall into two distinct groups with nearly opposite modal directions highlighted by the rose diagram (Fig. 7c). Foliation planes also have the opposite plunge and their direction is consistent with the current modes (Fig. 7 a). The mean current directions are computed as a mixture of 2 Von Mises distributions, which is necessary since we have two groups of directions and Von Mises distributions are unimodal. Calculations were performed using the R-package "movMF" (Hornik and Grün, 2014) and returned two independent distributions, the first with mean direction m=45.3° and concentration parameter k = 6.3, and a the second with mean direction m 227.4° and concentration parameter k = 2.2 (Fig. 7e). The current directions are nearly antipodal as expected for seasonally reversing monsoon-driven currents. In the set with P' < 1.1, the flow directions, the foliation planes and I_1 axis appear dispersed, probably because bottom currents were absent or too weak to produce a coherent directional pattern in elongated sediment particles (Fig. 7b and Fig. 7d). A Kuiper test for uniformity accepted the Null hypothesis at the 95% confidence level testifying that these directions do not have a preferential orientation. According to these observations stratigraphic intervals with larger P' indicate the presence of stronger bottom currents that flow alternatively toward NE and SW. The N-S components of the observed currents are interpreted as a deflection of equatorial zonal currents in the Inner Sea of the Maldives where bottom currents are forced to follow the sea floor morphology and the directions of the main channels. Inferred current directions are virtually identical to those of present-day bottom current data measured by acoustic Doppler profiler by Lüdmann et al. (2013).

The presence of bottom currents is not constant throughout the stratigraphic record. In fact the degree of anisotropy P' is generally very small in the lower part of the stratigraphic column (mean 1.05±0.03) and shows larger values (mean 1.22± 0.17) in the upper part with a sudden increase at about 168±2 m CSF-A, which corresponds to the top of Chron C3n.1n and an age of about 4.2 Ma (Fig. 8). The increase of anisotropy in the upper 168 m CSF-A is synchronous with a more gradual decrease of IRM intensity, which is indicative of a decreased concentration of magnetic minerals. The decrease of IRM intensity can be interpreted as a superimposed long-term trend with an acceleration starting at the depth of ~168 m CSF-A (Fig. 8b). No changes in the main lithological units were observed at this depth (Betzler et al., 2017), however the decreased concentration of magnetite is followed by deteriorated quality of the paleomagnetic measurements and decreased sedimentation rate in the upper part of Site U1467. From the sedimentological point of view, the decrease of IRM is interpreted as a consequence of changes in the sediment transport mechanism -controlled by wind driven currents- that transferred the sediments and the single-domain magnetite, possibly of biogenic origin, from the shallow platform to the deeper water of Site U1467 (Lüdmann et al., 2013). This process is modified by the increased monsoon strength starting at ~168 m CSF-A and the depocenter of drift deposits moving downstream. Regardless of the reason for the IRM decrease, the increased anisotropy can be associated with changes in sedimentation dynamics that lead to drift deposition and that has been related to the onset of strong modern monsoon system (Betzler et al., 2016b).

Our results suggest that starting from the lower Pliocene (ca. 4.2 Myr ago) the monsoon-related bottom currents became strong enough to significantly increase the degree of anisotropy and create a mostly transverse pattern in the sediments with large AIRM. Increased monsoon strength could qualitatively be explained with the onset of the intertropical convergence zones (ITCZ) to their present-day position. This implies a southern shift of the ITCZ south of the Himalayas and an increase in the latitudinal separation of the summer and winter ITCZ that moved the winter ITCZ south of the Maldives (e.g., Allen and Armstrong, 2012 and references therein). The Himalayas and Tibet have a primary influences on atmospheric circulation patterns and hence climate of the region. For this reason the surface uplift history of the Himalayan-Tibetan orogen has been suggested to be closely linked to the development of the Asian monsoon (Clift et al., 2008) and in fact, Tibetan plateau and Himalayan uplift is considered necessary for the presence of the strong present day monsoon (Prell and Kutzbach, 1997).

During the late Cenozoic the regional uplift may have occurred in two stages, one beginning in the Late Miocene, which probably led to the beginning of the drift deposition at 12.9 Ma (Betzler et al., 2016b), followed by a later Pliocene phase dated approximately from 5 to 2 Myr ago (Harrison et al, 1992; Zheng et al., 2000; An et al., 2001) that could have been recorded in Site U1467. Independent evidence supporting a coeval increase of monsoon intensity through enhanced precipitation, occurring at about 4 Ma, is given by the magnetic susceptibility record from ODP site 758, (Prell and Kutzbach, 1997, An et al., 2001), which is interpreted as the sea-level-mediated fluvial transport from the Ganges and other river systems draining the southern side of the Himalaya-Tibet plateau. Moreover, Zheng et al., (2000) interpret the increase in sedimentation rate and change in depositional facies from redbeds to upward-coarsening conglomerate and debris-flow deposits at the foot of the Kunlun Mountains as evidence for the uplift of the north-western Tibetan Plateau between 3.5 and 4.5 Ma. The timing of increased current strength in the Maldives platform is compatible with the beginning of the Pliocene uplift stage, and in fact this could mark precisely the beginning of climatic influence of the Pliocene Himalayan uplift at 4.2 Ma.

5. Conclusions

Paleomagnetic study of IODP Site U1467 provides a magnetic stratigraphy that gives an improved age model of the Pliocene portion of Site U1467 compensating for the scarcity of the biostratigraphic data in this time interval. This new age model can potentially be the basis for further astrochronological studies.

The analysis of the AIRM has shown evidence of bottom currents with alternating directions similar to the present-day currents. We found that the strength of the bottom currents inferred from the AIRM-corrected anisotropy degree P' increased suddenly at about 4.2 Myr ago. This is interpreted as the formation of stronger equatorial undercurrents as a consequence of increased monsoon strength.

A number of studies relate the strength of Asian monsoon to the uplift of the Himalayas and Tibetan plateau. We observe that the timing of the increase of bottom currents (4.2 Ma) coincides with the increase of fluvial transport to the Bay of Bengal and is compatible with the beginning of the Late Pliocene phase of Himalayan uplift, suggesting that is represents the Maldives record of the Late Pliocene uplift phase. In this case our age model gives a precise timing of this event.

Acknowledgments

The authors thank the crew of the JOIDES Resolution. Financial support for this research was provided by IODP-Italia and University of Urbino (DiSPeA) . Laboratory analyses were performed thanks to "Consorzio Interuniversitario di Magnetismo Naturale (CIMaN)". Two anonymous reviewers contributed to improve the manuscript.

Bibliography

1. An, Z., Kutzbach, J.E., Prell, W.L., Porter, S.C., 2001. Evolution of Asian monsoons and phased uplift of the Himalayan Tibetan plateau since Late Miocene times. Nature, 411, 62-66.
2. Allen, J.R.L., 1984. Sedimentary Structures: their Character and Physical Basis. Developments in Sedimentology, vol. 30A/B. Elsevier, Amsterdam. 593/663 pp.
3. Allen, M.B. and Armstrong, H.A., 2012. Reconciling the Intertropical Convergence Zone, Himalayan/Tibetan tectonics, and the onset of the Asian monsoon system, *Journal of Asian earth sciences.*, 44 . pp. 36-47.
4. Baas, J. H., Hailwood, E. A., McCaffrey, W. D., Kay, M. & Jones, R. 2007. Directional petrological characterisation of deep-marine sandstones using grain fabric and permeability anisotropy: Methodologies, theory, application and suggestions for integration. Earth- Science Reviews, 82, 101–142.
5. Besse, J., and Courtillot, V. 2002. Apparent and true polar wander and the geometry of the geomagnetic field over the last 200 Myr, *J. Geophys. Res.*, 107(B11), 2300, doi: 10.1029/2000JB000050.
6. Betzler C., Hübscher, C. Lindhorst S. , Reijmer J.J.R., Römer M, Droxler A.W. , Fürstenau J. and Lüdmann T., 2009, Monsoon-induced partial carbonate platform drowning (Maldives, Indian Ocean). Geology, 37(10): 867–870; doi: 10.1130/G25702A.1
7. Betzler, C., Fürstenau, J., Lüdmann, T., Hübscher, C., Lindhorst, S., Paul, A., Reijmer, J.J.G., and Droxler, A.W., 2013. Sea-level and ocean-current control on carbonate-platform growth, Maldives, Indian Ocean. *Basin Research*, 25(2):172–196.
8. Betzler, C.G., Eberli, G.P., Alvarez Zarikian, C.A., and the Expedition 359 Scientists, 2016. Expedition 359 Preliminary Report: Maldives Monsoon and Sea Level. International Ocean Discovery Program. http://dx.doi.org/10.14379/iodp.pr.359.2016
9. Betzler, C., G.P. Eberli, D. Kroon, J.D. Wright, P.K. Swart, B.N. Nath, C.A. Alvarez-Zarikian, et al. 2016(b). The Abrupt Onset of the Modern South Asian Monsoon Winds. *Scientific Reports* 6. https://doi.org/10.1038/srep29838.
10. Betzler, C., Eberli, G.P., Alvarez Zarikian, C.A., Alonso-García, M., Bialik, O.M., Blättler, C.L., Guo, J.A., Haffen, S., Horozal, S., Inoue, M., Jovane, L., Kroon, D., Lanci, L., Laya, J.C., Ling Hui Mee, A., Lüdmann, T., Nakakuni, M., Nath, B.N., Niino, K., Petruny, L.M., Pratiwi, S.D., Reijmer, J.J.G., Reolid, J., Slagle, A.L., Sloss, C.R., Su, X., Swart, P.K., Wright, J.D., Yao,

Z., and Young, J.R., 2017. Site U1467. *In* Betzler, C., Eberli, G.P., Alvarez Zarikian, C.A., and the Expedition 359 Scientists, *Maldives Monsoon and Sea Level*. Proceedings of the International Ocean Discovery Program, 359: College Station, TX (International Ocean Discovery Program). http://dx.doi.org/10.14379/iodp.proc.359.105.2017

11. Betzler, C., G.P. Eberli, D. Kroon, J.D. Wright, P.K. Swart, B.N. Nath, C.A. Alvarez-Zarikian, et al. 2018. Refinement of Miocene sea level and monsoon events from the sedimentary archive of the Maldives (Indian Ocean). *Progress in Earth and Planetary Science* 5:5 doi10.1186/s40645-018-0165-x
12. Clift, P.D., Hodges, K.V., Heslop, D., Hannigan, R., Van Long, H., Calves, G., 2008. Correlation of Himalayan exhumation rates and Asian monsoon intensity. Nature Geoscience, 1, 875-880.
13. Cleveland, W. S. (1979). Robust locally weighted regression and smoothing scatterplots. Journal of the American Statistical Association, 74, 829–836. doi: 10.1080/01621459.1979.10481038.
14. Cleveland, W. S., Grosse E. and Shyu W. M. (1992) Local regression models. Chapter 8 of Statistical Models in S eds J.M. Chambers and T.J. Hastie, Wadsworth & Brooks/Cole.
15. Felletti, F., Dall'Olio, E. and Muttoni G., 2016. Determining Flow Directions in Turbidites: An Integrated Sedimentological and Magnetic Fabric Study of the Miocene Marnoso Arenacea Formation (Northern Apennines, Italy). *Sedimentary Geology*. https://doi.org/10.1016/j.sedgeo.2016.02.009.
16. Gradstein, F. M., Ogg J.G., Mark D. Schmitz MD., and Ogg G.M., 2012. The Geologic Time Scale 2012. The Geologic Time Scale 2012. https://doi.org/10.1016/C2011-1-08249-8.
17. Hamilton, N., Rees, A.I., 1970. The use of magnetic fabric in paleocurrent estimation. In: Runcorn, S.K. (Ed.), Palaeogeophy- sics. Academic Press, New York, pp. 445–464.
18. Harrison, T. M., Copeland, P., Kidd, W. S. F. and Yin, A., 1992. Raising Tibet. Science 255, 1663-1670.
19. Harms, J.C., Southard, J.B., Walker, R.G., 1982. Structures and Sequences in Clastic Rocks. SEPM Short Course, vol. 9. 249 pp.
20. Hendry, H.E., 1976. The orientation of discoidal clasts in resedimented conglomerates, Cambro-Ordovician, Gaspé, eastern Quebec. Journal of Sedimentary Petrology 46, 48–55.
21. Hornik K., Grün B., 2014. movMF: AnRPackage for Fitting Mixtures of von Mises-

FisherDistributions. Journal of Statistical Software,58(10), 1–31. URLhttp://www.jstatsoft.org/v58/i10/

22.

23. Iskandar, I., Y. Masumoto, and K. Mizuno (2009), Subsurface equatorial zonal current in the eastern Indian Ocean, J. Geophys. Res., 114, C06005, doi:10.1029/2008JC005188.

24. Jackson, M., 1991. Anisotropy of magnetic remanence: A brief review of mineralogical sources, physical origins, and geological applications, and comparison with susceptibility anisotropy. PAGEOPH, 136: 1-28. https://doi.org/10.1007/BF00878885

25. Jelinek, V. 1981. "Characterization of the Magnetic Fabric of Rocks." Tectonophysics, 79, T63-T67, https://doi.org/10.1016/0040-1951(81)90110-4.

26. Johansson, C.E., 1964. Orientation of pebbles in running water: a laboratory study. *Geografiska Annaler* 45A, 85–112.

27. Kirschvink J. L., 1980. The least-squares line and plane and the analysis of palaeomagnetic data, *Geophysical Journal International*, 62, 3, 699–718, https://doi.org/10.1111/j.1365-246X.1980.tb02601.x

28. Knox, R. A. (1976), On a long series of measurements of Indian Ocean equatorial currents near Addu Atoll, Deep Sea Res. Oceanogr. Abstr., 23, 211–221.

29. Lurcock, P. C. and G. S. Wilson (2012), PuffinPlot: A versatile, user-friendly program for paleomagnetic analysis, Geochemistry, Geophysics, Geosystems, 13, Q06Z45, doi:10.1029/2012GC004098.

30. Lüdmann, T., Kalvelage, C., Betzler, C., Fürstenau, J., and Hübscher, C., 2013. The Maldives, a giant isolated carbonate platform dominated by bottom currents. *Marine and Petroleum Geology*, 43:326–340.

31. Lüdmann T., C. Betzler, G.P. Eberli, J. Reolid, J.J.G. Reijmer, C.R. Sloss, O.M. Bialik, C.A. Alvarez-Zarikian, M. Alonso-García, C.L. Blättler, J. A. Guo, S. Haffen, S. Horozal, M. Inoue, L. Jovane, D. Kroon, L. Lanci, J.C. Laya, A.LH. Mee, M. Nakakuni, B.N. Nath, K. Niino, L.M. Petruny, S.D. Pratiwi, A.L. Slagle, X. Su, P.K. Swart, J.D. Wright, Z. Yao, J.R. Young, 2018. Carbonate Delta Drift: A New Sediment Drift Type. Marine, Geology 401. https://doi.org/10.1016/j.margeo.2018.04.011

32. Nyadjro, E. S., and M. J. McPhaden (2014), Variability of zonal currents in the eastern equatorial Indian Ocean on seasonal to interannual time scales, J. Geophys. Res. Oceans, 119, 7969–7986, doi:10.1002/2014JC010380.

33. Novak, B., Housen, B., Kitamura, Y., Kanamatsu, T., and Kawamura, K., 2014. Magnetic Fabric Analyses as a Method for Determining Sediment Transport and Deposition in Deep Sea Sediments. Marine Geology. https://doi.org/http://dx.doi.org/10.1016/j.margeo.2013.12.001.

34. Potter, D. K., 2004. A Comparison of Anisotropy of Magnetic Remanence Methods -- a User's Guide for Application to Palaeomagnetism and Magnetic Fabric Studies. In Geological Society, London, Special Publications. https://doi.org/10.1144/GSL.SP.2004.238.01.03.

35. Prell, W.L., and Kutzbach, J.E., 1992. Sensitivity of the Indian monsoon to forcing parameters and implications for its evolution. Nature, 360:647-652.

36. Prell, W.L., and Kutzbach, J.E., 1997. The impact of Tibet-Himalayan elevation on the sensitivity of the monsoon climate system to changes in solar radiation. In Ruddiman, W.F. (Ed.), Tectonic Uplift and Climate Change: New York (Plenum), 172-203.

37. Rea, D.K., 1992. Delivery of Himalayan sediment to the northern Indian Ocean and its relation to global climate, sea level, uplift, and seawater strontium. In: Duncan, R.A., Rea, D.K., Kidd, R.B., von Rad, U., Weissel, J.K. (Eds.), Synthesis of Results from Scientific Drilling in the Indian Ocean. Geophysical Monograph, vol. 70. Am. Geophys. Union, Washington DC, pp. 387–402.

38. Reppin, J., F. A. Schott, J. Fischer, and D. Quadfasel (1999), Equatorial currents and transports in the upper central Indian Ocean: Annual cycle and interannual variability, J. Geophys. Res., 104, 15,495–15,514.

39. Rusnak, G.A., 1957. The orientation of sand grains under conditions of "unidirectional" fluid flow: 1. Theory and experiment. Journal of Geology 65, 384–409.

40. Schott, F., and J. P. McCreary (2001), The monsoon circulation of the Indian Ocean, Prog. Oceanogr., 51, 1–123.

41. Schwarzacher, W., 1963. Orientation of crinoids by current action. Journal of Sedimentary Petrology 33, 580–586.

42. Stephenson, A., Sadikun, S., Potter, D.K., 1986. A theoretical and experimental comparison of the anisotropy of magnetic susceptibility and remanence in rocks and minerals. Geophys. J. R. astr. Soc., 84: 185-200.

43. Taira, A. and Peter Scholle, A., 1979. Origin of Bimodal Sands in Some Modern Environments. Journal of Sedimentary Research. https://doi.org/10.1306/212F7847-

2B24-11D7-8648000102C1865D.

44. Tauxe, L., 2002. Paleomagnetic Principles and Practice. Modern Approaches in Geophysics. Vol. 17. New York: Springer.

45. Torsvik T.H., R. Van der Voo, U. Preeden, C. Mac Niocaill, B. Steinberger, P.V. Doubrovine, D.J.J. van Hinsbergen, M. Domeier, C. Gaina, E. Tohver, J.G. Meert, P.J.A. McCausland, L.R.M. Cocks, 2012. Phanerozoic polar wander, palaeogeography and dynamics, Earth-Science Reviews, 114, 325-368.

46. Wunsch, M. , Betzler, C. , Lindhorst, S. , Lüdmann, T. , Eberli, G. P. and Della Porta, G., 2017. Sedimentary dynamics along carbonate slopes (Bahamas archipelago). Sedimentology, 64: 631-657. doi:10.1111/sed.12317

47. Zheng, H., C. McAulay Powell, Z. An, J. Zhou, and G. Dong. 2000. Pliocene Uplift of the Northern Tibetan Plateau. Geology. https://doi.org/10.1130/0091-7613(2000)28<715:PUOTNT>2.0.CO;2.

Captions

Figure 1

Location map of IODP Site U1467.

Figure 2

Acquisition of isothermal remanent magnetization of representative samples from the investigated site (A) and the estimate of the density distribution of median destructive field of the natural remanent magnetization (B). Isothermal remanent magnetization acquisition shows that all samples are saturated at fields higher than 100-150 mT indicating the presence of low coercivity minerals. The low coercivity rules out the presence of relevant amounts of hematite or diagenetic iron-sulphides and suggests that magnetite (or maghemite) is the main magnetic mineral in the sediments. The histogram and the density distribution of the median destructive field has a mode of about 10 mT confirming that the natural remanent magnetization is carried by low-coercivity minerals.

Figure 3

Representative examples of vector plots of alternating field demagnetization of natural remanent magnetization. Stepwise demagnetization of natural remanent magnetization of sediments from Site U1467 shows generally a very small overprint, which is removed at a maximum field of 10-20 mT, followed by a linear path toward the origin that is interpreted as the characteristic remanent magnetization. Blue segments represent the direction of the characteristic remanent magnetization computed as the best-fit line of the selected demagnetization steps (shown in red).

Figure 4

Jelinek plot (Jelinek, 1981) illustrating the shape of anisotropy tensor (T) and corrected degree of anisotropy (P'). Symbol size is proportional to the intensity of isothermal remanent magnetization.

Figure 5

ChRM directions (Declination and Inclination) , maximum angular deviation and virtual geomagnetic pole latitude plotted against core depth (m CFS-A). The latitude of the virtual geomagnetic pole is computed from the declination and inclination in order to better interpret the geomagnetic polarities, which are reported in the left column as black and white intervals for normal and reversed polarity, respectively. The horizontal dashed lines indicate cores breaks and the small symbols in the left side of the VGP Latitude panel indicates the measured levels. The biostratigraphic events, core photographs and sedimentary units from Betzler et al. (2017) are also reported. Notice that the paleomagnetic inclinations are not significantly different from zero except for transitional directions, indicating an equatorial paleo-latitude of the site.

Figure 6

Paleomagnetic interpretation and age model of the studied portion of Site U1467. Shipboard biostratigraphic events are reported to provide the general age frame. The reversal polarity sequence, N1 to N6, from Site U1467 is shown in the right-vertical axis. The open circles connected by the red line represent the correlation of this polarity reversal sequence to the reference geomagnetic polarity scale on the horizontal upper axis.

Figure 7

A and B) Equal area projection of the main anisotropy axis I_1 and foliation planes for the specimens sets with P' ≥ 1.1 and P' < 1.1, respectively. I_1 axis are shown in different colours depending on their flow pattern. The set with P' ≥ 1.1, mostly taken above 168±2 m CSF-A, shows foliation planes imbricated along the current direction, in this case imbrications approximately toward NE and SW indicates currents flowing alternatively in these opposite directions. C and D) Current directions shows in the circular plots (dots) together with their rose diagram. The set with P' ≥ 1.1 shows two distinct modal values while the set with P' < 1.1 have uniformly distributed directions. E) Von Mises distributions and mean values (red arrows) for the set of current directions with P' ≥ 1.1.

Figure 8

Summary of anisotropy of isothermal remanent magnetization data versus depth. P' indicates the corrected anisotropy degree, the shape parameter T is illustrated with a colour code. The IRM is indicative of concentration of magnetic minerals. Data have been smoothed using the locally weighted regression method (Cleveland 1979, Cleveland et al., 1992) to illustrate the main trend. The 95% confidence level is shown by the grey band. The reversal polarity column provides a time frame and ties the age of the green band marking the shift toward higher anisotropy and lower IRM intensity to the top of chron C3n.1n.

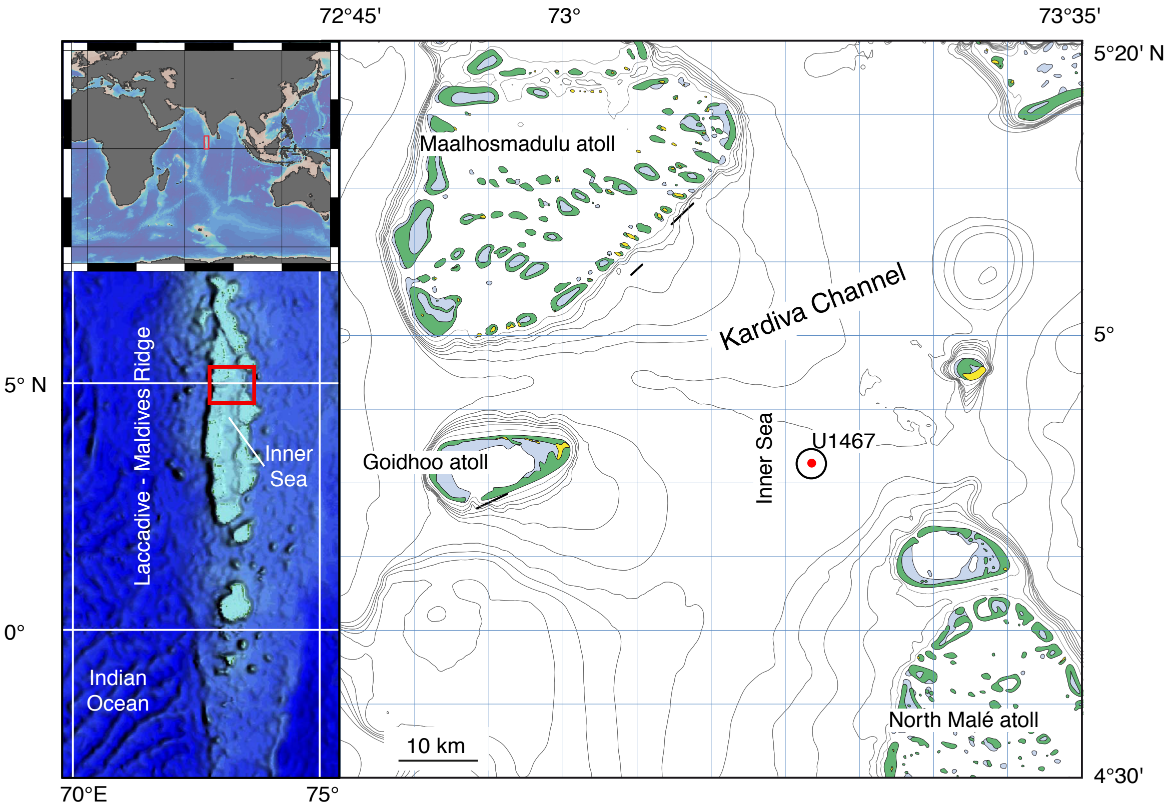

72°45'
73°
73°35'
5°20' N
5°
4°30'
5° N
0°
70°E
75°
Maalhosmadulu atoll
Kardiva Channel
Goidhoo atoll
Inner Sea
U1467
North Malé atoll
10 km
Laccadive - Maldives Ridge
Inner
Sea
Indian
Ocean

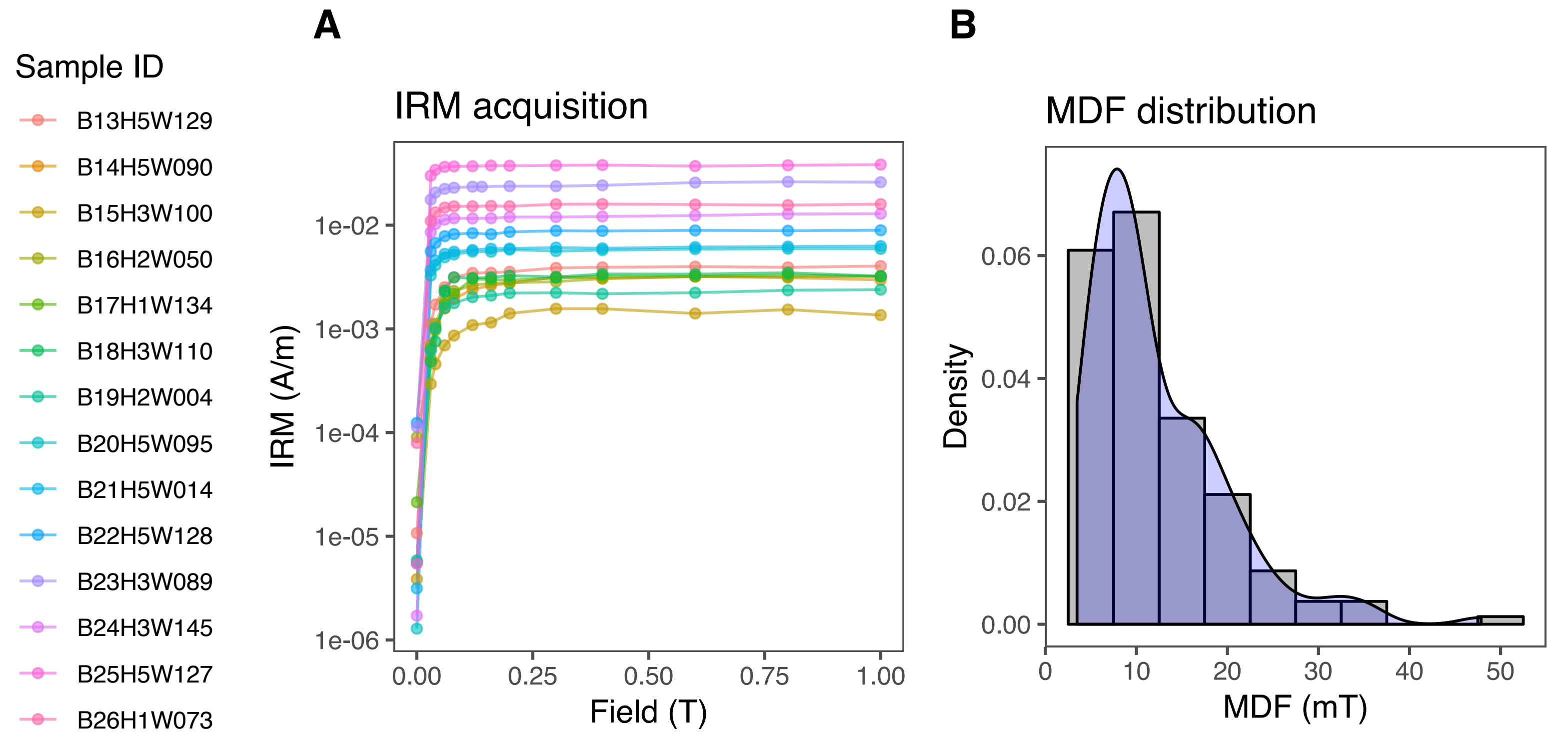
A
B
Sample ID
B13H5W129
B14H5W090
B15H3W100
B16H2W050
B17H1W134
B18H3W110
B19H2W004
B20H5W095
B21H5W014
B22H5W128
B23H3W089
B24H3W145
B25H5W127
B26H1W073
IRM acquisition
IRM (A/m)
1e-02
1e-03
1e-04
1e-05
1e-06
0.00
0.25
0.50
0.75
1.00
Field (T)
MDF distribution
Density
0.06
0.04
0.02
0.00
0
10
20
30
40
50
MDF (mT)

Sample: B13H3W098

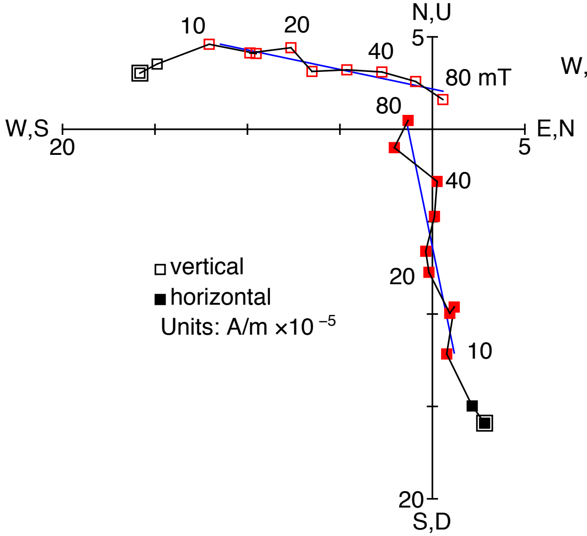

Sample: B15H3W100

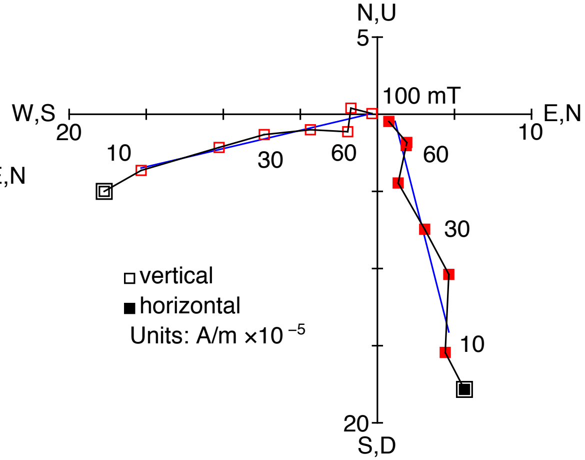

Sample: B20H6W017

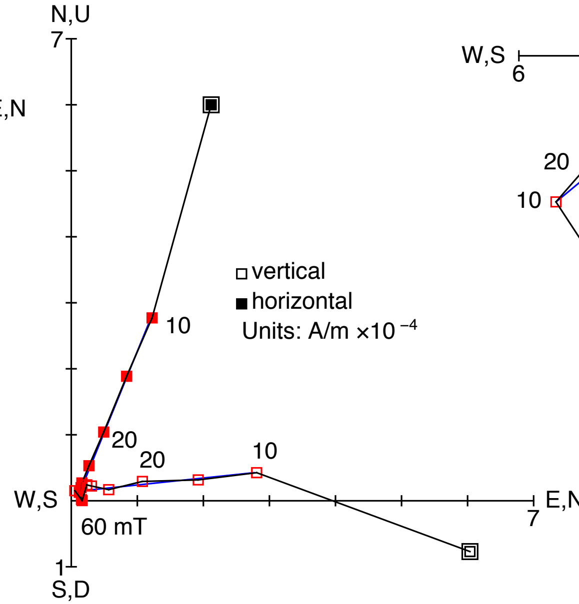

Sample: B21H2W123

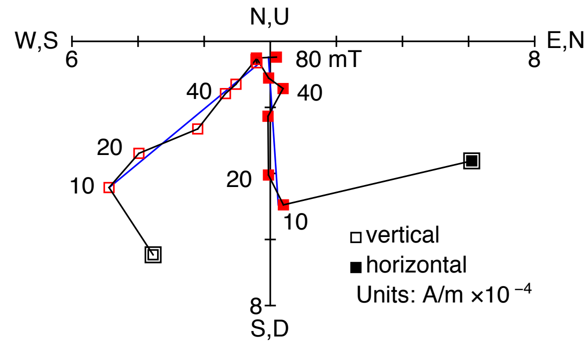

Sample: C16H4W048

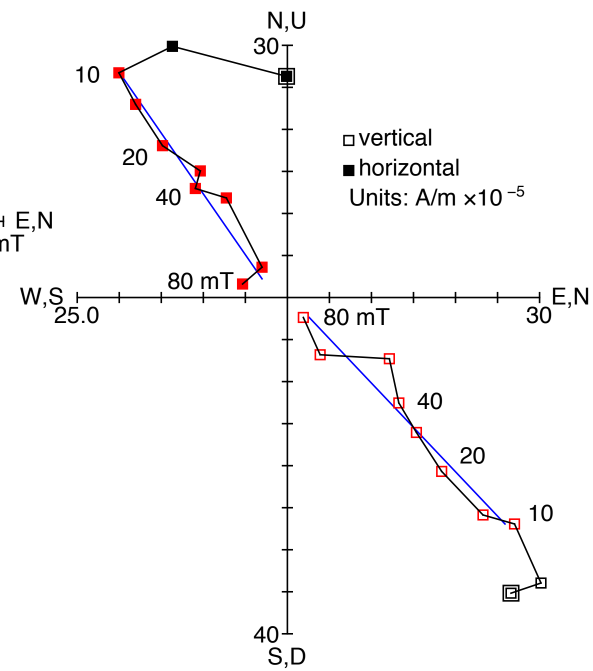

Sample: B26H3W080

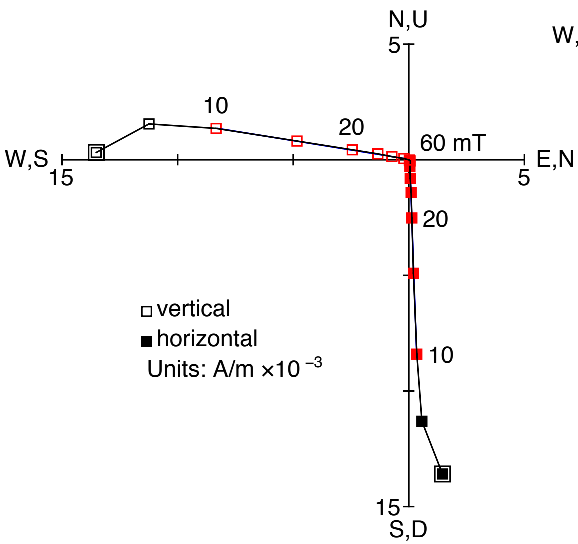

Sample: B33H3W069

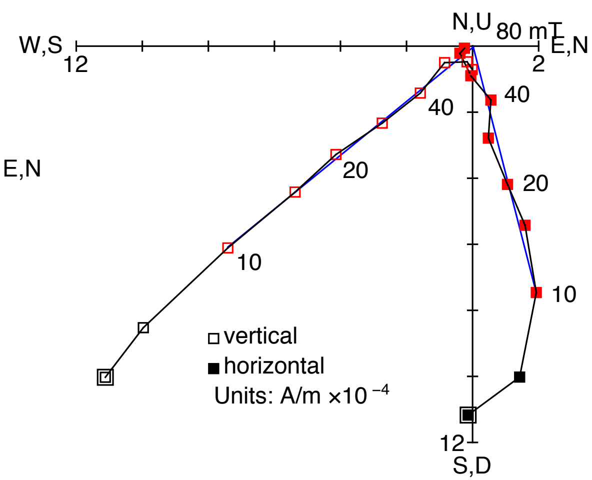

Sample: C15H3W147

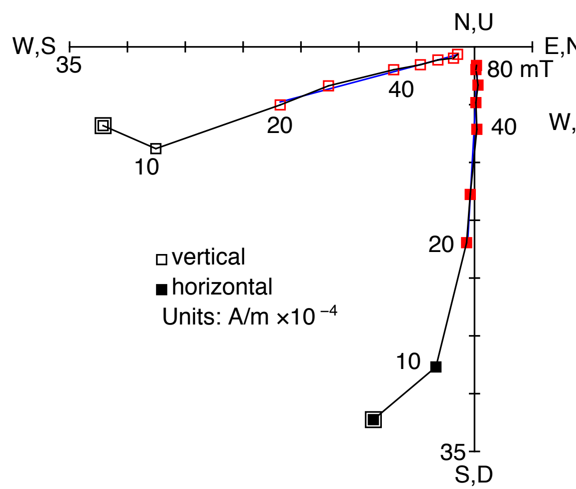

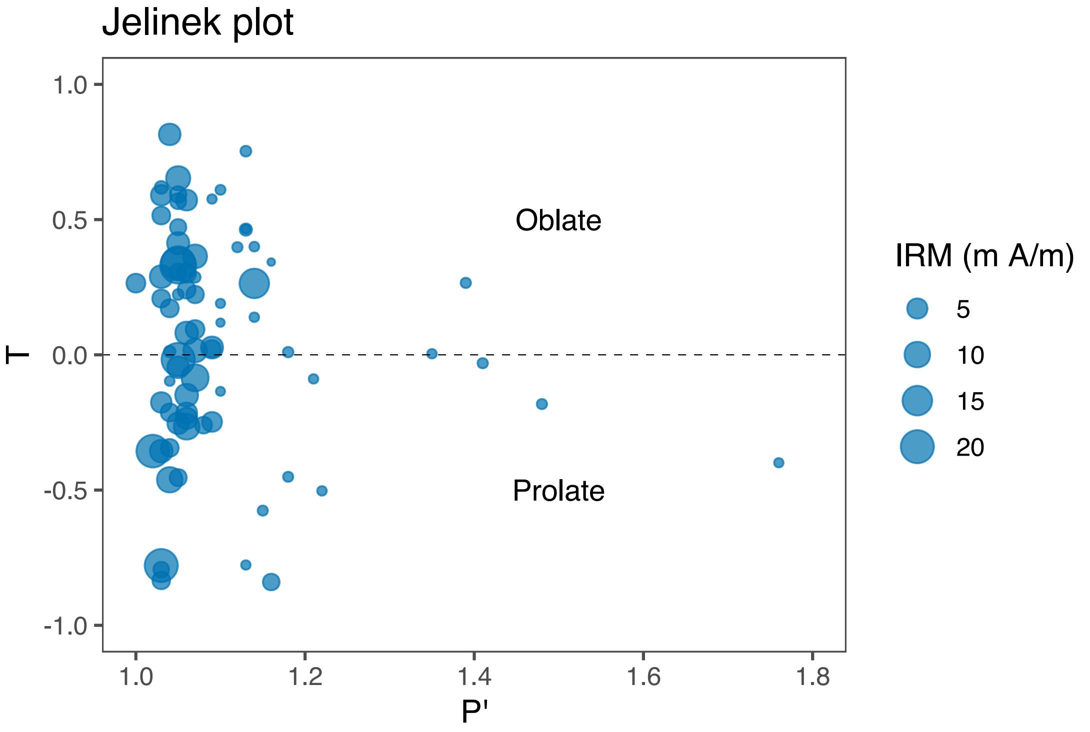
Jelinek plot
1.0
0.5
0.0
-0.5
-1.0
T
Oblate
Prolate
1.0
1.2
1.4
1.6
1.8
P'
IRM (m A/m)
5
10
15
20

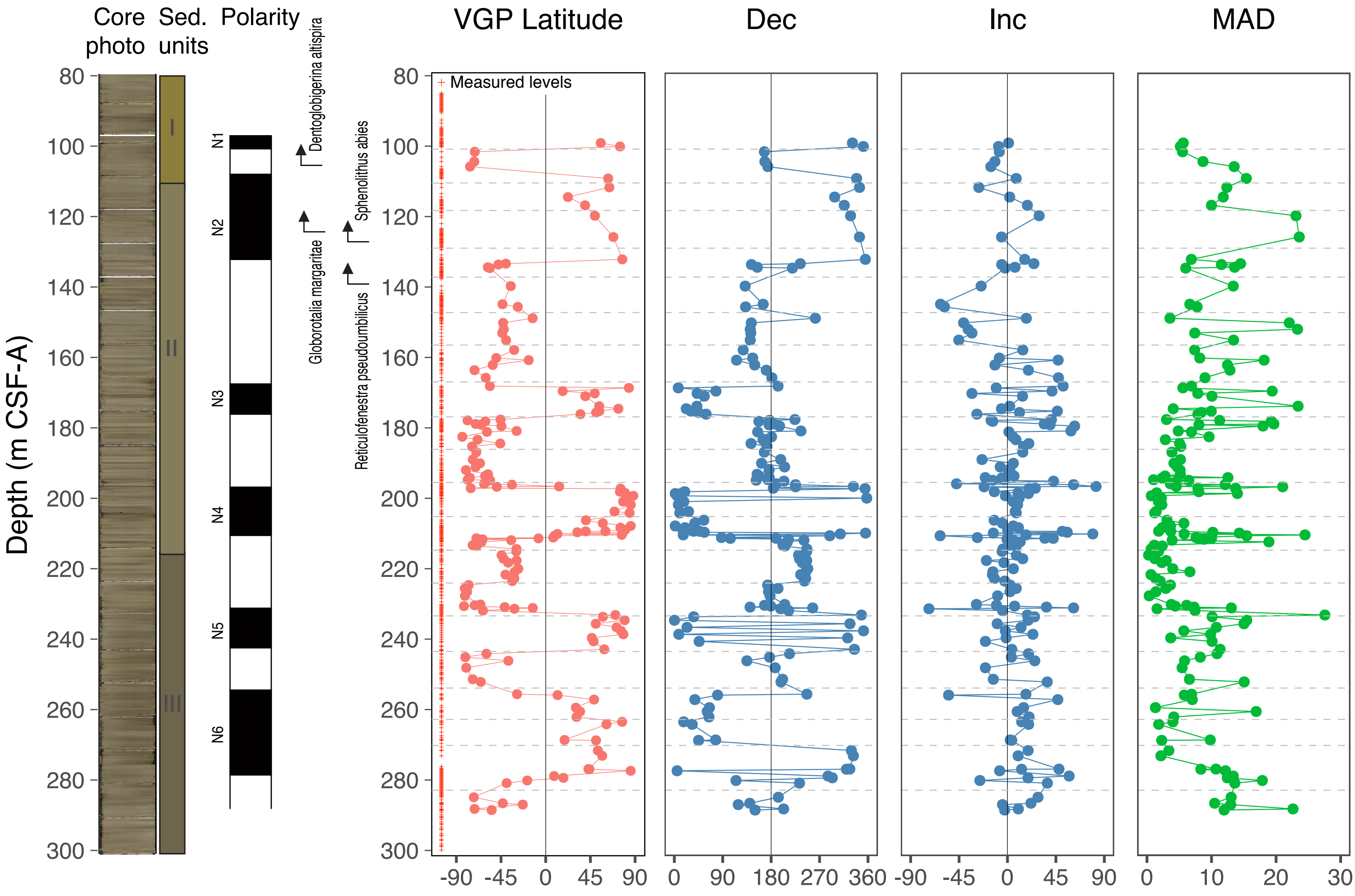

Core photo
Sed. units
Polarity
VGP Latitude
Dec
Inc
MAD
Depth (m CSF-A)
Measured levels
I
II
III
N1
N2
N3
N4
N5
N6
Dentoglobigerina altispira
Sphenolithus abies
Globorotalia margaritae
Reticulofenestra pseudoumbilicus
80
100
120
140
160
180
200
220
240
260
280
300
-90 -45 0 45 90
0 90 180 270 360
-90 -45 0 45 90
0 10 20 30

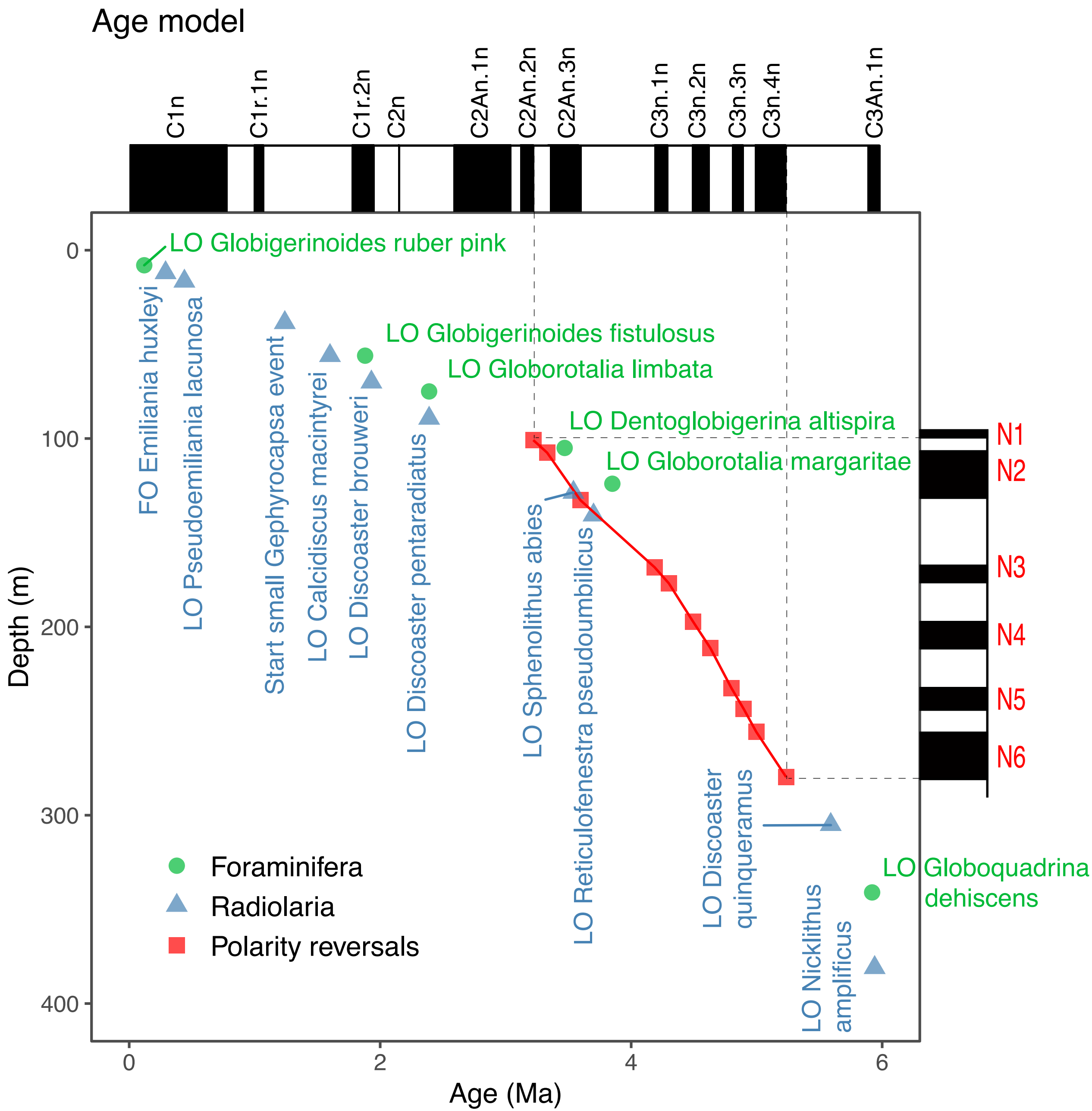

Age model
C1n
C1r.1n
C1r.2n
C2n
C2An.1n
C2An.2n
C2An.3n
C3n.1n
C3n.2n
C3n.3n
C3n.4n
C3An.1n
LO Globigerinoides ruber pink
FO Emiliania huxleyi
LO Pseudoemiliania lacunosa
Start small Gephyrocapsa event
LO Calcidiscus macintyrei
LO Discoaster brouweri
LO Globigerinoides fistulosus
LO Globorotalia limbata
LO Discoaster pentaradiatus
LO Dentoglobigerina altispira
LO Globorotalia margaritae
LO Sphenolithus abies
LO Reticulofenestra pseudoumbilicus
LO Discoaster quinqueramus
LO Nicklithus amplificus
LO Globoquadrina dehiscens
N1
N2
N3
N4
N5
N6
Foraminifera
Radiolaria
Polarity reversals
Depth (m)
0
100
200
300
400
Age (Ma)
0
2
4
6

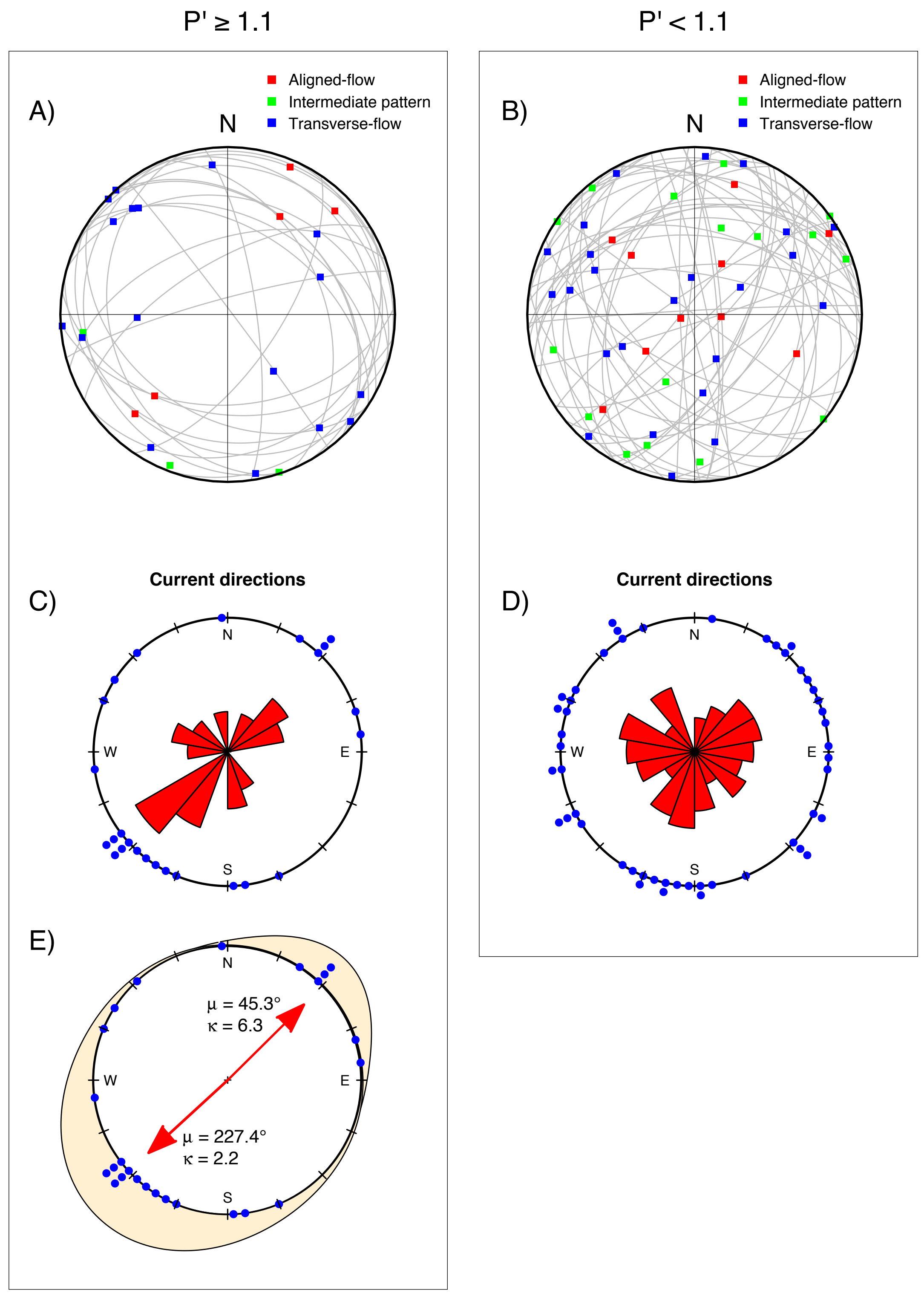

P' ≥ 1.1
P' < 1.1
A)
B)
Aligned-flow
Intermediate pattern
Transverse-flow
N
C)
D)
Current directions
N
E
S
W
E)
μ = 45.3°
κ = 6.3
μ = 227.4°
κ = 2.2

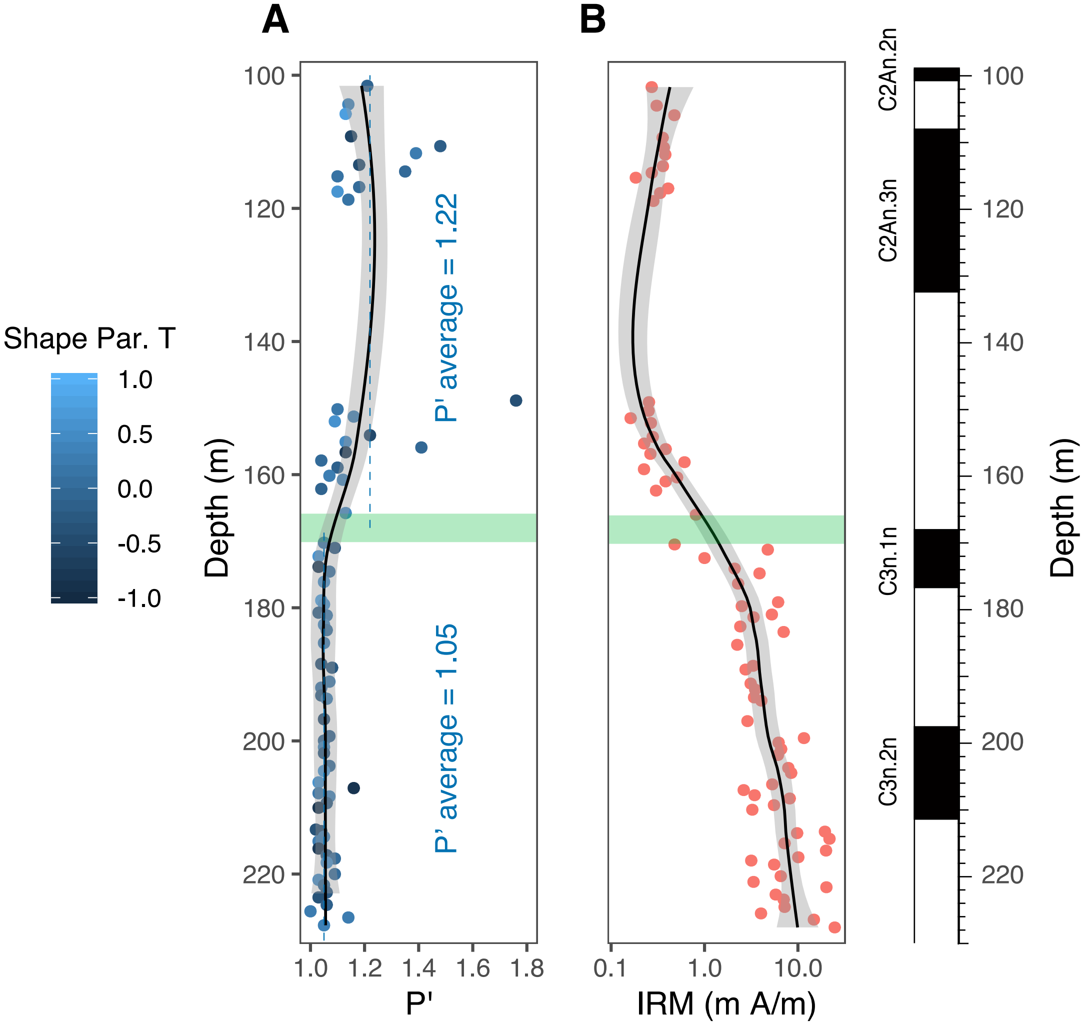

A
B
Shape Par. T
1.0
0.5
0.0
-0.5
-1.0
Depth (m)
P' average = 1.22
P' average = 1.05
P'
IRM (m A/m)
C2An.2n
C2An.3n
C3n.1n
C3n.2n

Table 1; Mean direction, Virtual Geomagnetic Pole position and paleo latitude of Site U1467 (the relatively low precision of the data is mostly a consequence of the poor azimuthal orientation of the cores).

Fisher Statistics	Dec = 5.7, Inc = 1.6, R = 121.91, k = 3.12, a_{95} = 7.2, N = 179
VGP	Lat = 82.9, Long = 198.5, dm_{95} = 7.2 dp_{95} = 3.6
Paleo Latitude	l = 0.8° , l_{+95} = 4.4°, l_{-95} = -2.8°

Table 2: Magnetostratigraphic reversals

Chron	Age (Ma)	Depth Top (m CSF-A)	Depth Bottom (m CSF-A)
C2An.2n Bottom	3.220	100.10	101.59
C2An.3n Top	3.330	105.81	109.18
C2An.3n Bottom	3.596	132.15	133.38
C3n.1.n Top	4.187	168.14	168.65
C3n.1n Bottom	4.300	176.11	177.64
C3n.2n Top	4.493	197.15	197.26
C3n.2n Bottom	4.631	211.15	211.36
C3n.3n Top	4.799	231.89	233.15
C3n.3n Bottom	4.896	242.89	244.14
C3n.4n Top	4.997	255.63	255.89
C3n.4n Bottom	5.235	279.39	280.14